



저작자표시-비영리-변경금지 2.0 대한민국

이용자는 아래의 조건을 따르는 경우에 한하여 자유롭게

- 이 저작물을 복제, 배포, 전송, 전시, 공연 및 방송할 수 있습니다.

다음과 같은 조건을 따라야 합니다:



저작자표시. 귀하는 원저작자를 표시하여야 합니다.



비영리. 귀하는 이 저작물을 영리 목적으로 이용할 수 없습니다.



변경금지. 귀하는 이 저작물을 개작, 변형 또는 가공할 수 없습니다.

- 귀하는, 이 저작물의 재이용이나 배포의 경우, 이 저작물에 적용된 이용허락조건을 명확하게 나타내어야 합니다.
- 저작권자로부터 별도의 허가를 받으면 이러한 조건들은 적용되지 않습니다.

저작권법에 따른 이용자의 권리는 위의 내용에 의하여 영향을 받지 않습니다.

이것은 [이용허락규약\(Legal Code\)](#)을 이해하기 쉽게 요약한 것입니다.

[Disclaimer](#)

이학박사 학위논문

**Electrical Properties of MoS₂ Field-Effect
Transistors Treated with Organic Thiol
Molecules**

유기 싸이올 분자 처리를 통한 이황화 몰리브덴
전계 효과 트랜지스터의 전기적 변화에 대한 연구

2019 년 2 월

서울대학교 대학원

물리·천문학부

조 경 준

Electrical Properties of MoS₂ Field-Effect Transistors Treated with Organic Thiol Molecules

유기 싸이올 분자 처리를 통한 이황화 몰리브덴
전계 효과 트랜지스터의 전기적 변화에 대한 연구

지도 교수 이 탁 희

이 논문을 이학박사 학위논문으로 제출함

2019년 1월

서울대학교 대학원

물리·천문학부 물리학 전공

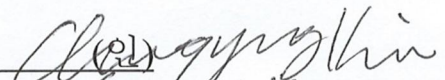
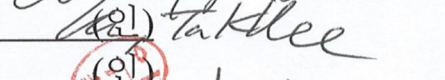
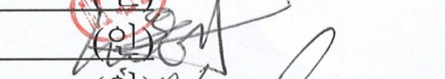
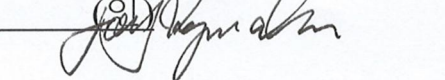

조 경 준

조경준의 이학박사 학위논문을 인준함

2019년 1월

위 원 장
부위원장
위 원
위 원
위 원

_____ 김 창 영
_____ 이 탁 희
_____ 이 규 철
_____ 민 흥 기
_____ 안 중 현

(인) 
(인) 
(인) 
(인) 
(인) 

Abstract

Electrical Properties of MoS₂ Field Effect Transistors Treated with Organic Thiol Molecules

Kyungjune Cho

Department of Physics and Astronomy
Seoul National University

Two-dimensional (2D) materials, such as graphene and transition metal dichalcogenides (TMDs), has been widely gained much attention due to their novel features. Because graphene has no electric bandgap which is generally required to be used as a semiconductor, TMDs have been proposed as the promising 2D-layered materials for future device applications. Among these TMDs, molybdenum disulfide (MoS₂) has been widely studied due to its direct bandgap of 1.9 eV as a single layer and indirect bandgap of 1.3 eV as a bulk crystal. Hence, numerous studies have been conducted to explore the applications of MoS₂. However, due to the 2D nature of MoS₂, interfaces of MoS₂-based devices can heavily influence the electrical and optical properties of MoS₂. Therefore, understanding how interfaces affect the characteristics of MoS₂ and various interface engineering strategies are demanded for the emerging nano-electronic devices.

In this regards, first, I investigated the electrical properties of MoS₂ field-effect transistors (FETs) influenced by environment. The MoS₂ devices were fabricated using the electron-beam lithography method. Then, the electrical properties of the devices were characterized under various measurement conditions, such as varying gate bias stress time, gate sweep rate, gate sweep range, and environment. I observed a certain gate bias stress instability behaviors and interpreted them by field-induced adsorptions of oxygen

molecules or water molecules originated from gate-bias stress effect. Hence, the gate bias stress effect was not observed in vacuum condition.

Secondly, I conducted a research on the electrical and optical properties of MoS₂ FETs with thiol molecule treatment. Organic thiol molecules tend to latch on the sulfur vacancies on the surface of the MoS₂. After thiol molecule treatment, the current level and carrier concentration were dramatically decreased, even though subthreshold swing (SS) value of the device, which is related to the surface defects, was not considerably changed. This phenomena is ascribed to reduction in the concentration of sulfur vacancies by the thiol molecule treatment.

Finally, I proposed a new approach for modifying charge injection properties of MoS₂ FETs. I inserted thiol molecules between metal electrodes and MoS₂ channel to reduce the charge injection barrier and remove interfacial states which cause Fermi level pinning. The charge injection properties of thiol inserted MoS₂ FETs showed an ohmic-like behavior even at the low temperature (~80 K), whereas those of untreated MoS₂ FETs showed Schottky-like behavior even at the room temperature (~300 K). Fabrication of asymmetric MoS₂ devices was also feasible by employing this strategy to only one contact.

Keywords: Two dimensional materials, Transition metal dichalcogenides, Molybdenum disulfide, Electrical characteristics, Gate bias stress effects, Interface engineering, Thiol molecule treatment

Student Number: 2012-20388

List of Contents

Abstract	i
List of Contents	iii
List of Figures	vi
Chapter 1. Introduction	1
1.1. Brief introduction of TMDs and MoS ₂	1
1.2. Electrical properties of MoS ₂ influenced by surface	2
1.3. Electrical properties of MoS ₂ influenced by metal contact	3
1.4. Electrical properties of MoS ₂ FETs treated with organic thiol molecules	3
1.5. Outline of this thesis	4
References	6

Chapter 2. Electrical Properties of MoS₂ FETs Influenced by

Environment

2.1. Introduction	8
2.2. Experiments	10
2.2.1. Device fabrication process	10
2.2.2. Electrical characterization	12
2.3. Results and discussions	12
2.3.1. Electrical characteristics of MoS ₂ FETs	12
2.3.2. Threshold voltage instability of MoS ₂ FETs under gate bias stress	14
2.3.3. Gate bias stress time dependence	17
2.3.4. Gate voltage sweep rate, sweep range dependence	18
2.3.5. Environmental condition dependence	21

2.3.1. Energy band schematic	22
2.4. Conclusion	24
References	25

Chapter 3. Electrical Properties of MoS₂ FETs with Thiol

Molecule Surface treatment.....	28
3.1. Introduction.....	28
3.2. Experiments	30
3.2.1. Device fabrication process	30
3.2.2. Thiol molecule treatment.....	31
3.3. Results and discussions	32
3.3.1. Electrical properties of MoS ₂ FETs	32
3.3.2. Electrical properties of MoS ₂ FETs with thiol molecule treatment.....	35
3.3.3. Optical properties of MoS ₂ FETs with thiol molecule treatment	41
3.3.4. Thickness and surface area dependence	45
3.3.5. Energy band schematic	47
3.4. Conclusion	48
References	49

Chapter 4. Electrical Properties of MoS₂ FETs with Contact

Treatment by Thiol Molecule.....	52
4.1. Introduction.....	52
4.2. Experiments	54
4.2.1. Device fabrication process with inserted thiol molecules.....	54
4.2.2. Characterization of deposited thiol-molecules	56
4.2.3. Activation energy extraction.....	57
4.2.4. Contact resistance extraction by using Y-function method.....	57
4.3. Results and discussions	58

4.3.1. HRTEM and EELS analysis	58
4.3.2. XPS analysis.....	60
4.3.3. The effect of the thiol-molecule inserted at the contact region	62
4.3.4. Electrical characterization of MoS ₂ FETs with asymmetrix contact	66
4.3.5. Energy band schematics of asymmetric devices	69
4.4. Conclusion	70
References	72
Chapter 5. Summary	74
국문초록(Abstract in Korean).....	76
감사의 글	78

List of Figures

Chapter 2.

Figure 2.1 Schematics illustrating the device fabrication procedures. Adapted from Cho et al.

Figure 2.2 (a) AFM image and cross-sectional profile. (b) Optical images of a MoS₂ nano-sheet (left) before and (right) after the device fabrication. Adapted from Cho et al.

Figure 2.3 (a) The schematic of the MoS₂ FET. An optical image of a real device is also shown. (b) I_{DS} - V_G curve measured at a fixed $V_{DS} = 0.1$ V in vacuum. The inset shows I_{DS} - V_{DS} for different V_G . Adapted from Cho et al.

Figure 2.4 (a, b) I_{DS} - V_G curves (“Pre-stress”) measured before the gate bias stress, and 100 consecutive I_{DS} - V_G curves right after (a) +35 V gate bias stress and (b) -35 V gate bias stress was applied for 300 sec. Data were measured in ambient conditions. (c) The shift of the threshold voltage (ΔV_{Th}) for each measurement with respect to the value of the Pre-stress curve. Adapted from Cho et al.

Figure 2.5 (a, b) I_{DS} - V_G curves measured in ambient conditions after (a) +35 V and (b) -35 V gate bias stress was applied for different stress duration times. (c) The shift in the threshold voltage (ΔV_{Th}) for each measurement with respect to the value for the initial curve (“0 s” curve). The inset is the plot made on the logarithmic scale of stress time. Adapted from Cho et al.

Figure 2.6 (a, c) I_{DS} - V_G curves measured in ambient conditions with different gate bias sweep rates ranging from 8 V/s to 0.1 V/s. The gate bias was swept (a) from +35 V to -35 V and (c) from -35 V to +35 V. (b, d) The threshold voltage (V_{Th}) at each measurement for different sweep rates for gate bias swept (b) from +35 V to -35 V and (d) from -35 V to +35 V. Insets in (b, d) are plots made as the linear scale of sweep rate. Adapted from Cho et al.

Figure 2.7 (a) The hysteresis I_{DS} - V_G curves of double sweep (from -35 V to +35 V and then back to -35 V) at different gate bias sweep rates measured in the ambient environment. (b) The hysteresis I_{DS} - V_G curves with different gate bias sweep range at a fixed gate bias sweep rate of 0.1 V/s in ambient. Adapted from Cho et al.

Figure 2.8 (a) I_{DS} - V_G curves measured in vacuum after -35 V gate bias stress was

applied for different stress duration time. (b) I_{DS} - V_G curves measured in vacuum during the gate bias sweep from +35 V to -35 V with different gate bias sweep rates. Adapted from Cho et al.

Figure 2.9 The schematics of the energy band diagram at $V_G = 0$ V in the ambient environment when (a) no gate bias stress, (b) positive gate bias stress, and (c) negative gate bias stress is applied. Adapted from Cho et al.

Chapter 3.

Figure 3.1 Schematics illustrating the device fabrication procedures. Adapted from Cho et al.

Figure 3.2 (a) Schematic images of the fabrication process of MoS₂ FETs with the optical images shown under the each schematic image. (b) Schematic images of a MoS₂ FET before (left) and after (right) the alkanethiol molecule treatment. Adapted from Cho et al.

Figure 3.3 (a) I_{DS} - V_G curve measured at a fixed $V_{DS} = 0.5$ V with logarithmic scale. The inset shows I_{DS} - V_G curves with linear scale. (b) I_{DS} - V_{DS} curves measured with V_G varying from 40 to -60 V. Adapted from Cho et al.

Figure 3.4 (a) I_{DS} - V_G curves measured before and after the hexadecanethiol treatment with logarithmic scale. The inset shows I_{DS} - V_G curves with linear scale. (b) I_{DS} - V_{DS} curves measured before and after the hexadecanethiol treatment. (c) The contour plots of I_{DS} as a function of V_G and V_{DS} before (left) and after (right) the hexadecanethiol treatment. Adapted from Cho et al.

Figure 3.5 (a) I_{DS} - V_G curves measured before and after hexadecanethiol treatment with varying temperature from 80 to 320 K. (b) Carrier concentration and threshold voltage of a MoS₂ FET as a function of temperature acquired before and after the hexadecanethiol treatment. (c) Mobility and SS value of a MoS₂ FET as a function of temperature acquired before and after the hexadecanethiol treatment. Adapted from Cho et al.

Figure 3.6 (a) The optical image of a MoS₂ flake that was used for Raman and PL studies. (b) The Raman spectra measured from a circled region marked in (a) before and after the hexadecanethiol treatment. (c) The Raman mapping image of E_{2g}^1 mode

and A_{1g} mode before (left) and after (right) the hexadecanethiol treatment. We added dotted lines to indicate the MoS_2 flakes in this figure. Adapted from Cho et al.

Figure 3.7 (a) PL peak position mapping image of the MoS_2 flake shown in Figure 4(a) before (left) and after (right) the hexadecanethiol treatment. (b) PL spectra measured from a circled region before and after the hexadecanethiol treatment. We added dotted lines to indicate the MoS_2 flakes in this figure. Adapted from Cho et al.

Figure 3.8 (a) Difference in channel currents measured before (I_{Pristine}) and after (I_{After}) the hexadecanethiol treatment for ten MoS_2 FET devices with different layer thicknesses (height) of the MoS_2 channel. (b) Difference channel currents before and after hexadecanethiol treatment as a function of the surface area to volume ratio of the MoS_2 channel film. The blue dashed lines were added to demonstrate the dependence of the channel current difference on the MoS_2 channel's height or surface area to volume ratio. Adapted from Cho et al.

Figure 3.9 The schematics of the energy band diagram at $V_G = 0$ (a) before and (b) after the alkanethiol molecule treatment. Adapted from Cho et al.

Chapter 4.

Figure 4.1. (a) Schematic images of the device fabrication process. (b) Optical images of the MoS_2 FETs during the fabrication process. (c) Schematics of the decanethiol (DT) and perfluorodecanethiol (PFDT) molecule. Adapted from Cho et al.

Figure 10 (a) (left) HRTEM image of untreated MoS_2 sample, (middle) EELS data along the orange line in the HRTEM image at position 1, 2, and 3 and (right) magnified EELS data at position 2. b) (left) HRTEM image of DT-treated MoS_2 sample, (middle) EELS data along the orange line in the HRTEM image at position 1, 2, and 3 and (right) magnified EELS data at position 2. c) (left) HRTEM image of PFDT-treated MoS_2 sample, (middle) EELS data along the orange line in the HRTEM image at position 1, 2, and 3 and (right) magnified EELS data at position 2. Adapted from Cho et al.

Figure 4.3 (a) XPS mapping image and optical image of (top) untreated, (middle) PFDT-treated, and (bottom) DT-treated MoS_2 . Blue dots are the position where the Mo peak was observed in XPS, purple dots represents S, green dots represents C, and orange dots represents F. b) XPS data of untreated and thiol-treated MoS_2 . Adapted from Cho et al.

Figure 4.4 (a) Output curves with varying temperature from 80 K to 300 K of (top) untreated, (middle) DT-treated, and (bottom) PFDT-treated MoS₂ FETs at fixed gate bias. (b) (top) Contact and (bottom) energy band schematic for (left) untreated and (right) thiol-treated MoS₂. Adapted from Cho et al.

Figure 4.5 (a) Optical images of asymmetric MoS₂ FETs during the fabrication process. (b) Output curves at different gate bias conditions at fixed temperature. The drain electrode is DT treated and the source electrode is untreated. (c) Output curves at different temperature conditions at a fixed gate bias. The drain electrode is DT treated and the source electrode is untreated. (d) Output curves at different temperature conditions at a fixed gate bias. The source electrode is DT treated and the drain electrode is untreated. (e) Extracted activation energies of untreated, DT-treated, PFDT-treated, and HDT-treated MoS₂ FETs at different gate bias conditions. Red region represents “thermionic emission dominant” and blue region represents “field emission dominant”. (f,g) Rectification ratio at V_{DS} of -3 V and 3 V in (f) different gate bias conditions at a fixed temperature and at (g) different temperature conditions at a fixed gate bias. Adapted from Cho et al.

Figure 4.6 (a) Schematics of (left) device structures and (right) energy band diagram for asymmetric MoS₂ FETs. (b,c) Energy band diagram for (b) positively and (c) negatively biased source-drain condition. (d,e) Energy band diagram for (d) positively and (e) negatively biased gate condition. Adapted from Cho et al.

This work is dedicated to my loving wife Gahyun and our family.

Chapter 1. Introduction

1.1. Brief introduction of TMDs and MoS₂

Recently, transition metal dichalcogenides (TMDs) which are representative two-dimensional (2D) materials having variable electronic bandgap depending on the layer thickness have been widely studied due to their unique properties.[1-6] Single-layer TMD can be achieved by using various exfoliation methods due to the relatively weak van der Waals (vdW) interaction between layers. Also, large-area synthesis of layered TMDs is possible by using molecular beam epitaxy (MBE) or chemical vapor deposition (CVD) methods. Aforementioned, numerous researches on the application of 2D-layered TMDs have been extensively conducted due to their interesting properties, such as having good electronic properties, the direct bandgap of monolayer TMDs, interesting magnetic properties or physical properties.[1-6] TMDs denoted by MX₂ are composed of transition metal(M) and chalcogens(X). Depending on the combination of M and X, the TMD also can have numerous characteristics, such as semi-metallic, semiconducting or superconducting properties.

Especially, molybdenum disulfide (MoS₂), which is one of the representative n-type semiconducting TMD materials, has been spotlighted due to its charming properties. Unlike graphene, bulk crystal MoS₂ has an indirect bandgap of 1.2 eV and monolayer MoS₂ has a direct bandgap of 1.9 eV, which gives an attractive property in optoelectronics device applications.[7-15] Moreover, the development of large area

synthesis or liquid exfoliation methods facilitates rapid progress in MoS₂ device applications in various research fields.

1.2. Electrical properties of MoS₂ influenced by surface

2D-MoS₂ flakes have a large surface to volume ratio due to their 2D layered structure. Therefore, electronic or optoelectronic properties of MoS₂ heavily depend on their interfaces or surface environments. [16-19] Commonly, interfaces of the TMD based devices can be classified into three different types: 1) interfaces between TMDs and vacuum/air generally denoted by surfaces, 2) interfaces between TMDs and top/bottom dielectric layers, and 3) interfaces between TMDs and metal electrodes generally denoted by contacts. The environmental conditions of these three types of interfaces hugely influence on electrical and optoelectrical characteristics of MoS₂ devices. In case of MoS₂ based field-effect transistor (FET) devices, oxygen molecules or water molecules can reduce device performance, adsorbed at the surface of MoS₂. [20,21] The large electronegativity value of oxygen molecules can allow them to capture electrons at the surface of MoS₂. Late et al found that the hysteresis window of single layer MoS₂ FET have become larger when the room humidity (RH) increased. [20] If RH increase, more water molecules can capture the carriers, leading reduction in current level. As well as humidity, Park et al reported that oxygen environment could degrade the performance of MoS₂ devices. [21] It was observed that reduced device performance under oxygen environments while considerable degradation of electrical properties was not observed under nitrogen environment. In addition, on the surface of MoS₂, there are native defects, such as sulfur atoms or sulfur mono-vacancies which can play important roles in the electrical properties of MoS₂. [22-24] Hence, understanding how surface effects on

electrical characteristics of MoS₂ is required to modulate properties of MoS₂ for future applications.

1.3. Electrical properties of MoS₂ influenced by a metal contact

Furthermore, interfacial characteristics between metal electrodes and MoS₂ also can effects on electrical properties of MoS₂, determining charge injection characteristics.[25,26] To realize fabrication of the high-performance device, understanding contact properties of 2D TMDs and achieving better charge injection characteristics are required. Especially, it is found that interfacial defects located between TMD and metal electrodes could influence in charge injection properties of the TMD based devices.[25,26]. According to McDonnel et al, near the defect sites of MoS₂, huge tunneling current through the defects were observed by using a scanning tunneling microscope (STM).[27] In addition, those metal-like defects of MoS₂ contributed to Fermi level pinning, according to Bampoulis et al.[28] It is found that the extracted Schottky barrier height between MoS₂ and metal tips of STM weakly depends on the work function of metal tips which means that MoS₂ barely follows Schottky-Mott rule. Therefore, delivering good contact properties without using contact engineering strategies is hard to be realized.

1.4. Electrical properties of MoS₂ FETs treated with organic thiol molecules

Variety kinds of TMD have diverse material properties, such as metallic (e.g. NbS₂), semi-metallic (e.g. WTe₂), semiconducting (e.g. MoS₂, WSe₂) and superconducting (e.g. TaS₂, NbSe₂).[1] Combination of different chemical components facilitates designing, synthesis, and development of novel organic materials which have various properties. Hence, surface or interface engineering by using organic materials could be one of the most promising approaches to modulating electrical and optoelectrical properties of TMDs. Combination of various TMDs and various organic treatment will provide huge opportunities to understand material properties and how these material properties can be modified and functionalized for future applications.

Like silane and thiol molecules, self-assembled monolayers (SAMs) have been widely used for surface or interface engineering.[19] It has been known that thiol molecules can form SAM on the surface of noble metals and silane molecules can form SAM on the surface of an oxide layer such as Al₂O₃, SiO₂. Molecules which consist SAM generally have 3 components; (i) linker group located at the bottom, (ii) alkyl backbone located at the middle and (iii) end group located at the top. Each component of molecules can adopt various organic group to consist of a single molecule. Therefore, there could be numerous kinds of molecules which can be used for defect or interface engineering of TMDs. Also, it is reported that organic thiol molecules which have sulfur containing group can passivate those sulfur vacancies or remove sulfur adatoms of MoS₂ which have been considered as an important factor in determining device performance.[29 - 34]

1.6. Outline of This Thesis

This thesis mainly focuses on the electrical characterization of MoS₂ FETs devices

with organic interface treatment. In chapter 2, I discuss the electrical properties of MoS₂ FETs influenced by environmental condition via their surface. Analyses of gate bias stress effects on threshold voltage instabilities of MoS₂ FETs under various measurement conditions are also discussed. In chapter 3, I discuss the electrical and optical characteristics of untreated and thiol-treated MoS₂ FETs, varying thickness of MoS₂ channel and surface area/volume ratio. In chapter 4, I discuss electrical properties of MoS₂ FETs with contact treatment by using different types of organic thiol molecules which have the different molecular length or different direction of intrinsic electric dipole moments. Finally, chapter 5 summaries this thesis and suggests some future directions.

References

- [1] Sangwan, V. K.; Hersam, M. C.; *Annu. Rev. Phys. Chem.* **2018**, *69*, 299
- [2] Mas-Balleste, R.; Gomez-Navarro, C.; Gomez-Herrero, J.; Zamora, F.; *Nanoscale*, **2011**, *3*, 20
- [3] Chhowalla, M.; Jena, D.; Zhang, H.; *Nat. Rev. Mater.* **2016**, *1*, 1
- [4] Allain, A.; Kang, J.; Banerjee, K.; Kis, A.; *Nat. Mater.* **2015**, *14*, 1195
- [5] Wang, Q. H.; Kalantar-Zadeh, K.; Kis, A.; Coleman, J. N.; Strano, M. S.; *Nat. Nanotechnol.* **2012**, *7*, 699
- [6] Xia, F.; Wang, H.; Xiao, D.; Dubey, M.; Ramasubramaniam, A.; *Nat. Photon.* **2014**, *8*, 899
- [7] B. Radisavljevic, A. Radenovic, J. Brivio, V. Giacometti, A. Kis, *Nat. Nanotechnol.* **2011**, *6*, 147.
- [8] Q. H. Wang, K. Kalantar-Zadeh, A. Kis, J. N. Coleman, M. S. Strano, *Nat. Nanotechnol.* **2012**, *7*, 699.
- [9] K. F. Mak, C. Lee, J. Hone, J. Shan, T. F. Heinz, *Phys. Rev. Lett.* **2010**, *105*, 136805.
- [10] D. Xiao, G.-B. Liu, W. Feng, X. Xu, W. Yao, *Phys. Rev. Lett.* **2012**, *108*, 196802.
- [11] Y. Yoon, K. Ganapathi, S. Salahuddin, *Nano Lett.* **2011**, *11*, 3768.
- [12] D. Jariwala, V. K. Sangwan, L. J. Lauhon, T. J. Marks, M. C. Hersam, *ACS Nano* **2014**, *8*, 1102.
- [13] Y. Zhan, Z. Liu, S. Najmaei, P. M. Ajayan, J. Lou, *Small* **2012**, *8*, 966.
- [14] C.-H. Lee, G.-H. Lee, A. M. v. d. Zande, W. Chen, Y. Li, M. Han, X. Cui, G. Arefe, C. Nuckolls, T. F. Heinz, J. Guo, J. Hone, P. Kim, *Nat. Nanotechnol.* **2014**, *9*, 676.
- [15] M. Amani, D.-H. Lien, D. Kiriya, J. Xiao, A. Azcatl, J. Noh, S. R. Madhvapathy, R. Addou, S. KC, M. Dubey, K. Cho, R. M. Wallace, S.-C. Lee, J.-H. He, J. W. Ager III, X. Zhang, E. Yablonovitch, A. Javey, *Science* **2015**, *350*, 1065.
- [16] Wang, H.; Yuan, H.; Hong, S. S.; Li, Y.; Cui, Y.; *Chem. Soc. Rev.* **2015**, *44*, 2664.
- [17] Zhang, X.; Shao, Z.; Zhang, X.; He, Y.; Jie, J.; *Adv. Mater.* **2016**, *28*, 10409.
- [18] Zhao, Y.; Xu, K.; Pan, F.; Zhou, C.; Zhou, F.; Chai, Y.; *Adv. Funct. Mater.* **2017**, *27*, 1603484.
- [19] Lee, W. H.; Park, Y. D.; *Adv. Mater. Interfaces* **2018**, *5*, 1700316

- [20] Late, D. J.; Liu, B.; Matte, R.; Dravid, V. P.; Rao, C. N. R.; *ACS Nano*, **2012**, *6*, 5635.
- [21] Park, W.; Park, J.; Jang, J.; Jeong, H.; Cho, K.; Hong, S. C.; Lee, T.; *Nanotechnology* **2013**, *24*, 095202
- [22] Forster, A.; Gemming, S.; Seifert, G.; Tomanek, D.; *ACS Nano*, **2017**, *11*, 9989.
- [23] Qiu, H.; Xu, T.; Wang, Z.; Ren, W.; Nan, H.; Ni, Z.; Chen, Q.; Yuan, S.; Miao, F.; Song, F.; Long, G.; Shi, Y.; Sun, L.; Wang, J.; Wang, X.; *Nat. Commun.* **2013**, *4*, 2642.
- [24] Zhang, X.; Liao, Q.; Liu, S.; Kang, Z.; Zhang, Z.; Du, J.; Li, F.; Zhang, S.; Xiao, J.; Liu, B.; Ou, Y.; Liu, X.; Gu, L.; Zhang, Y.; *Nat. Commun.* **2017**, *8*, 15881.
- [25] M. Farmanbar, G. Brocks, *Phys. Rev. B.* **2015**, *91*, 161304.
- [26] M. Farmanbar, G. Brocks, *Adv. Electron. Mater.* **2016**, *2*, 1500405.
- [27] Park, J. H.; Sanne, A.; Guo, Y.; Amani, M.; Zhang, K.; Movva, H. C. P.; Robinson, J. A.; Javey, A.; Robertson, J.; Banerjee, S. K.; Kummel, A. C.; *Sci. Adv.* **2017**, *3*, e1701661.
- [28] Bampoulis, P.; Bremen, v. R.; Yao, Q.; Poelsema, B.; Zandvilet, H. J. W.; Kai, S.; *ACS Appl. Mater. Interfaces* **2017**, *9*, 19278.
- [29] M. Makarova, Y. Okawa, M. Aono, *J. Phys. Chem. C* **2012**, *116*, 22411.
- [30] C. G. Wiegenstein, K. H. Schulz, *J. Phys. Chem. B* **1999**, *103*, 6913.
- [31] S. L. Peterson, K. H. Schulz, *Langmuir* **1996**, *12*, 941.
- [32] X. Chen, N. C. Berner, C. Backes, G. S. Duesberg, A. R. McDonald, *Angew. Chem.* **2016**, *55*, 5803.
- [33] D. M. Sim, M. Kim, S. Yim, M.-J. Choi, J. Choi, S. Yoo, Y. S. Jung, *ACS Nano* **2015**, *9*, 12115.
- [34] S. Bertolazzi, S. Bonacchi, G. Nan, A. Pershin, D. Beljonne, P. Samori, *Adv. Meter.* **2017**, *29*, 1606760.

Chapter 2. Electrical Properties of MoS₂ FETs Influenced by Environment

In this chapter, we will discuss about the gate bias stress effects on electrical characteristics of MoS₂ FETs. We investigated the gate bias stress effects of multi-layered MoS₂ field effect transistors with a back-gated configuration. The electrical stability of the MoS₂ FETs can be significantly influenced by the electrical stress type, relative sweep rate, and stress time in an ambient environment. Specifically, when a positive gate bias stress was applied to the MoS₂ FET, the current of the device decreased and its threshold shifted in the positive gate bias direction. In contrast, with a negative gate bias stress, the current of the device increased and the threshold shifted in the negative gate bias direction. The gate bias stress effects were enhanced when a gate bias was applied for a longer time or when a slower sweep rate was used. These phenomena can be explained by the charge trapping due to the adsorption or desorption of oxygen and/or water on the MoS₂ surface with a positive or negative gate bias, respectively, under an ambient environment. This study will be helpful in understanding the electrical-stress-induced instability of the MoS₂-based electronic devices and will also give insight into the design of desirable devices for electronics applications.

2.1. Introduction

Two-dimensional (2D) nanomaterials with layered structures, such as graphene, are of considerable interest as promising materials for next-generation nanoelectronic device applications because of their unique properties and the ability to easily fabricate complex structures.[1,2] Among the layered materials, molybdenum disulfide (MoS₂) has recently attracted a lot of attention due to its intriguing electrical and optical properties compared to the substantial limitations of graphene in electronic transistors.[3,4]

Unlike graphene, which does not have a bandgap, bulk MoS₂ is a semiconductor with an indirect bandgap of 1.2 eV, and single-layer MoS₂ is a semiconductor with a direct bandgap of 1.8 eV.[5,6] Furthermore, MoS₂ has other excellent characteristics such as optical sensitivity and mechanical flexibility.[7-10] Accordingly, there have been considerable efforts into fabrication and characterization of MoS₂-based field effect transistors (FETs), sensing devices, memory devices, and logic circuits for future electronics and optoelectronics.[4,11-18] For example, single-layer MoS₂ transistors with a high on/off ratio of 10⁸ have recently been demonstrated using HfO₂ as the top gate dielectric.[4] Additionally, multi-layer MoS₂ transistors exhibiting high mobility (>100 cm²/Vs), near-ideal subthreshold swing (~70 mV/decade), and robust current saturation over a large voltage window have also been demonstrated.[18]

Despite these merits, large variations in the transport properties of MoS₂ FET devices due to extrinsic effects, such as absorption of oxygen and/or water from the environment, can result in limitations for exploring their intrinsic properties and overall stability.[19-22] Late *et al.* showed that the hysteresis effects of MoS₂ FET devices measured under an ambient environment were presumably due to extrinsic/environmental effects, especially absorption of moisture on the surface.[21] Qiu *et al.* showed that because the MoS₂ FET devices were sensitive to oxygen in the ambient environment, exposure to ambient conditions dramatically reduced the on-state current due to the additional scattering centers at the defect sites of MoS₂ caused by chemisorption.[22] They also demonstrated that vacuum annealing could effectively remove the adsorbates and reversibly recover the FET device performance.[22] Although there have been a number of reports on MoS₂ FET devices, the FET device stability under electrical stress has not yet been fully investigated. Understanding the electrical-stress-induced stability is

very important in MoS₂-based FETs for developing appropriate device operation schemes for use in practical electronic devices.

Here, we investigated the electrical-stress-induced instability of multi-layered MoS₂ FETs with a back-gated configuration under ambient condition. For example, we studied the device's characteristics in response to a positive or negative gate bias stress (± 35 V). The current of the device decreased (increased) and its threshold shifted in the positive (negative) gate bias direction with positive (negative) gate bias stress. We also studied the device's characteristics with different gate bias stress times, different gate bias sweep rates, and different gate sweep ranges. We compared the gate bias stress effects of the device in the ambient environment and in a vacuum.

2.2. Experiments

2.2.1. Device fabrication process

Figure 2.1 explains the device fabrication procedure. (1) First, we prepared 100-nm-thick SiO₂ on highly p⁺⁺ doped Si substrate that can be used as back gate. (2) Next, the MoS₂ flakes were exfoliated from a bulk MoS₂ crystal (SPI supplier, USA) by micromechanical exfoliation method. After we transferred the MoS₂ flakes on the substrate, we used an optical microscope to find MoS₂ nano-sheets which can be made to MoS₂ FETs. After finding proper MoS₂ nano-sheets, we measured the height of the MoS₂ nano-sheet using atomic force microscopy (AFM). (3) Then, we spin-coated MMA (8.5) MMA (9% concentration in ethyl lactate) with 4000 rpm for 50 sec. And we baked the sample at 180°C for one minute and 30 sec. (4) Next, the PMMA 950K (5% concentration in anisole) was spin-coated with 4000 rpm for 50 sec. And the sample was baked with 180°C for one minute and 30 sec. (5) The

electrode pattern was made by using an electron beam lithography (JSM-6510, JEOL). The pattern development was done with MIBK:IPA (1:3) solution for development time of 50 sec. (6) After development, we deposited Ti(10-nm-thick)/Au(100-nm-thick) as source and drain electrodes by using an electron beam

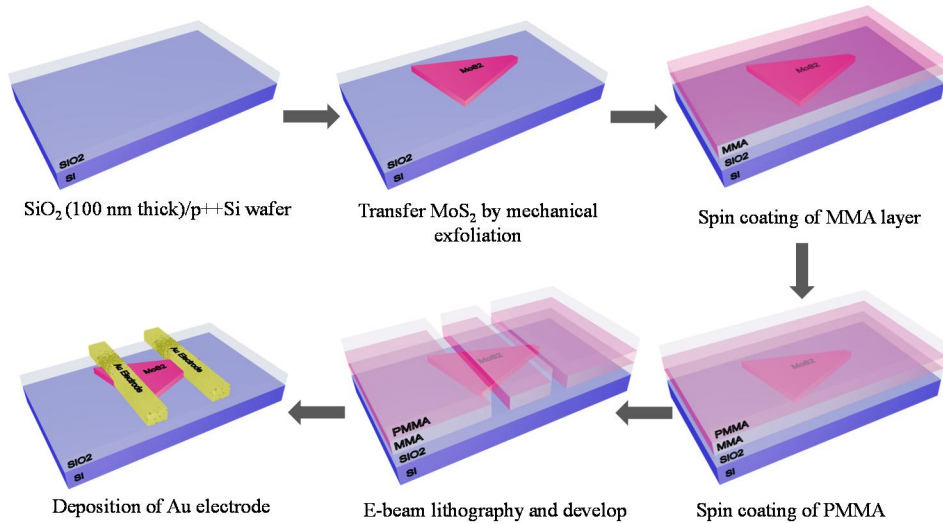


Figure 2.1 Schematics illustrating the device fabrication procedures.

evaporator.

Figure 2.2 shows the AFM image of a multi-layer MoS₂ nano-sheet. Cross-sectional profile across the line (red) marked in the AFM image is also shown. This particular MoS₂ nano-sheet has ~4.5 nm height, which corresponds to ~7 layers (the MoS₂ interlayer distance is ~6.5 Å). Figure 2.2(b) shows the optical images of a real MoS₂ nano-sheet before and after the device fabrication.

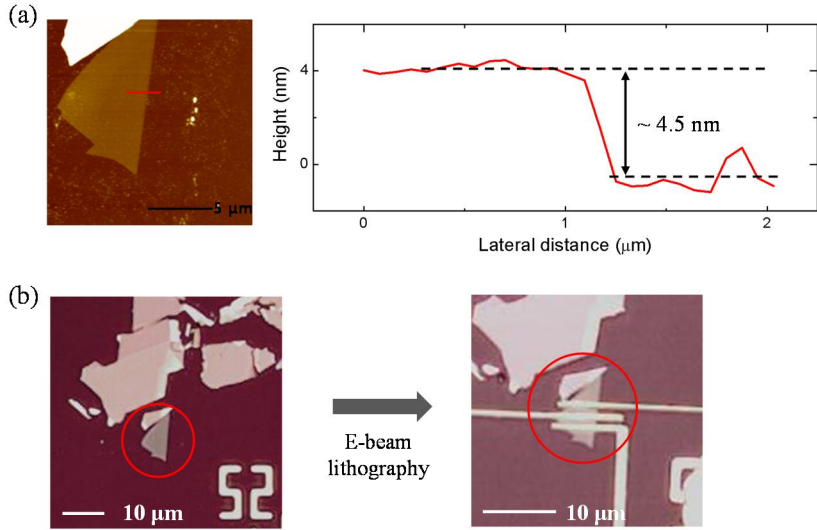


Figure 2.2 (a) AFM image and cross-sectional profile. (b) Optical images of a MoS₂ nano-sheet (left) before and (right) after the device fabrication

2.2.2. Electrical characterization

The electrical characteristics of the device were measured using a semiconductor parameter analyzer (HP 4145B) in a probe station (JANIS Model ST-500). Between each measurements, we waited about an hour before each measurement to ensure that the device fully recovered from the previous gate bias stress. We confirmed that the data were fully recovered; in other words, the measured data were almost the same after waiting an hour for all gate bias stresses.

2.3. Results and Discussions

2.3.1. Electrical characteristics of MoS₂ FETs

The MoS₂ flakes used in this study were prepared by the micromechanical exfoliation of a bulk MoS₂ crystal (purchased from SPI Supplier, USA). The exfoliated MoS₂ flakes were transferred to a 100-nm-thick SiO₂ layer on a highly doped p⁺⁺ Si

substrate that can be used as a back gate. After the MoS₂ flakes were transferred to the substrate, we located a suitable MoS₂ nano-sheet that was a few-layers thickness using an optical microscope. Then, to fabricate a MoS₂ FET device, the MoS₂ nano-sheet was patterned using electron beam lithography. After patterning, Au (100-nm-thick)/Ti (10-nm-thick) was deposited as the source and drain electrodes using an electron beam evaporator. Using these methods, we made three MoS₂ FET devices. However, for the systematic study and comparison, all the data presented in this study were from one device.

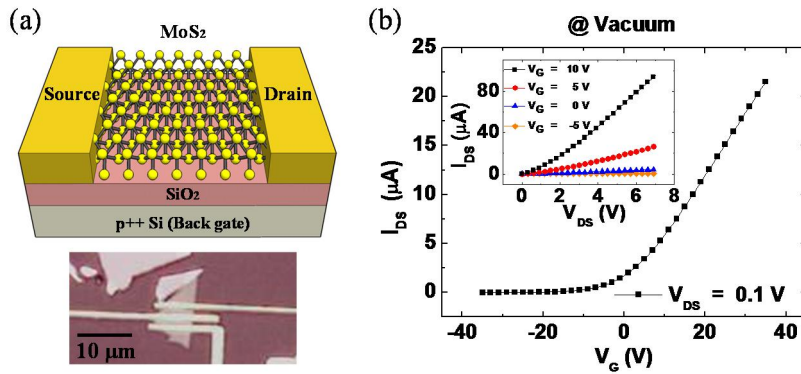


Figure 2.3 (a) The schematic of the MoS₂ FET. An optical image of a real device is also shown. (b) I_{DS} - V_G curve measured at a fixed $V_{DS} = 0.1$ V in vacuum. The inset shows I_{DS} - V_{DS} for different V_G .

Figure 2.3 (a) shows a schematic of a MoS₂ FET with an optical image of the real device used in this study. Figure 2.3(b) displays the representative transfer characteristics (source-drain current *versus* gate voltage, I_{DS} - V_G) measured at a fixed source-drain voltage ($V_{DS} = 0.1$ V). The inset of Figure 2.3(b) shows the output characteristics (source-drain current *versus* source-drain voltage, I_{DS} - V_{DS}) measured at different gate voltages ($V_G = 10, 5, 0,$ and -5 V). These data were measured in vacuum ($\sim 5.6 \times 10^{-5}$ torr). The device exhibited n-channel FET behavior because positive gate voltages increased the

current. From the transfer characteristics (Figure 2.3(b)), we estimated a field-effect mobility (μ) of $\sim 25.7 \text{ cm}^2/\text{Vs}$ using the following formula, $\mu = [dI_{DS}/dV_G] \times [L/(WC_iV_{DS})]$, [23] where $W = 6.3 \text{ }\mu\text{m}$ is the channel width, $L = 0.9 \text{ }\mu\text{m}$ is the channel length, and $C_i = \epsilon_0\epsilon_r/d \sim 3.5 \times 10^{-4} \text{ F/m}^2$ is the capacitance between the active layer and the back gate per unit area. Here, ϵ_r is the dielectric constant of SiO_2 (~ 3.9), ϵ_0 is the vacuum permittivity, and d is the SiO_2 thickness (100 nm). Previous studies have reported that the mobility of single-layer MoS_2 FETs is in the range from 0.1 to $\sim 200 \text{ cm}^2/\text{Vs}$. [4,18,19,24,25]

2.3.2. Threshold voltage instability of MoS_2 FETs under gate bias stress

We investigated the threshold voltage instability for the MoS_2 FET device under various gate bias stresses. To investigate the effect of the gate bias stress on the electronic properties of the device, we first applied a constant gate bias for 300 sec, and then we measured 100 transfer characteristic curves consecutively. Figures 2.4(a) and 2.4(b) display these repeated measurement results. First, the data were obtained (black curve, denoted as “Pre-stress”), then a constant +35 V (Figure 2.4(a)) or -35 V (Figure 2.4(b)) gate bias stress was applied for 300 sec, and finally, 100 consecutive data points were measured. After the positive gate bias stress, the source-drain current decreased significantly and the threshold voltage of the device shifted in the positive gate bias direction (see the data labeled “1^{sb}” in Figure 2.4(a)).

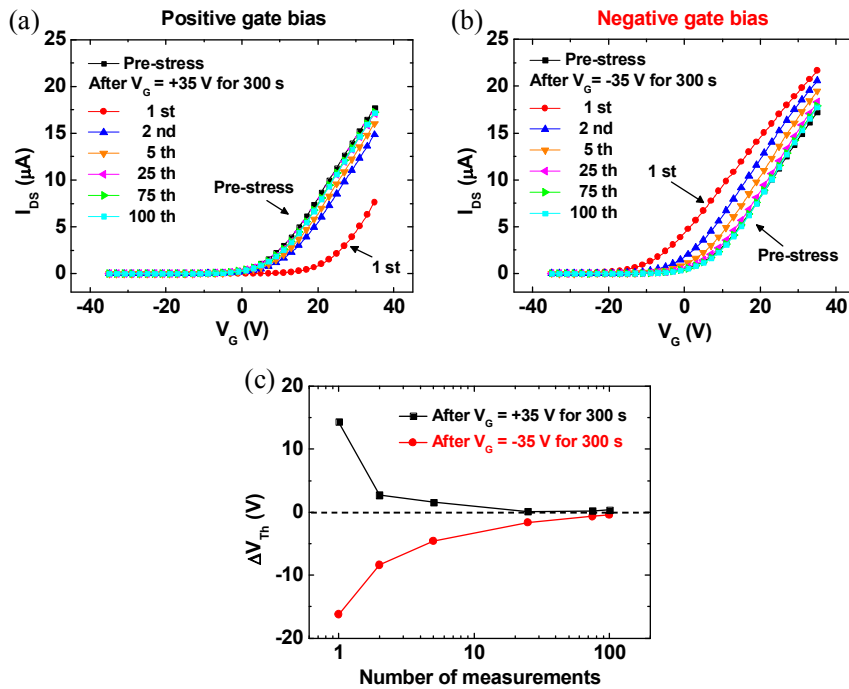


Figure 2.4 (a, b) I_{DS} - V_G curves (“Pre-stress”) measured before the gate bias stress, and 100 consecutive I_{DS} - V_G curves right after (a) +35 V gate bias stress and (b) -35 V gate bias stress was applied for 300 sec. Data were measured in ambient conditions. (c) The shift of the threshold voltage (ΔV_{Th}) for each measurement with respect to the value of the Pre-stress curve.

Then, the current gradually increased and the threshold voltage shifted in the negative gate bias direction, and eventually, the curve approached the original state (Pre-stress curve). In contrast, for the negative gate bias stress, the current increased and the threshold voltage shifted in the negative gate bias direction (see the data labeled “1st” in Figure 2.4(b)). Then, the current gradually decreased and the threshold voltage shifted in the positive gate bias direction, and similar to the positive gate bias stress, the curve returned to the original state (Pre-stress curve). Figure 2.4(c) shows the shift in the

threshold voltage at each measurement with respect to the value for the Pre-stress curve. Here, the threshold voltage is the value of the gate bias when the channel just begins to allow significant current to flow; we determined the threshold voltage from x (gate voltage)-axis intercept obtained from the linear fitting of the linear parts of the characteristic transfer curves.[23,26] With V_{Th} determined, we also estimated the carrier density of the device.

These phenomena (Figure 2.4) can be attributed to charge trapping due to the adsorption of oxygen and/or water in an ambient environment at defect sites on the MoS₂ surface.[19,20,22] Charge trapping under a positive gate bias stress can be enhanced by an increase in the adsorption of oxygen and/or water at the MoS₂ channel surface due to the increase in electrons caused by the positive gate bias. The charge trapping results in a decrease in the electrical conductance and causes the threshold voltage shifts in the positive gate bias direction. The electrons trapped on the MoS₂ surface can be released by applying a negative gate bias, which results in an increase in the conductance, and the threshold voltage shifts toward the negative gate bias direction. Similar behaviors have been observed in other types of nanoelectronic devices made with ZnO nanowires, InGaZnO(IGZO) films, and graphene.[27-33] Unlike such materials-based FETs, the threshold voltage instability in Si-based FETs can be explained mainly in terms of defect state creation and charge trapping effect at the interface between channel layer and dielectric layer under electrical stresses.[34-36] In our experiments, the adsorption/desorption of oxygen and water molecules on the MoS₂ surface under ambient environment starts to play dominant roles in the electrical transport properties of MoS₂ FETs.

2.3.3 Gate bias stress time dependence

We also investigated the effect of the gate bias stress time on the same device in ambient conditions. Figure 2.5(a) presents the transfer characteristic data (at $V_{DS} = 0.1$ V) of the device obtained right after we applied a constant +35 V gate bias for different gate bias stress times that varied from 0 to 500 sec with a fixed gate bias sweep rate of 8 V/s. The inset of Figure 2.5(a) shows the logarithmic plot. For example, the data labeled “10 s” were obtained after we applied a +35 V gate bias for 10 sec. We waited about an hour before each measurement to ensure that the device fully recovered from the previous gate bias stress. We confirmed that the data were fully recovered. Please see the two “0 s” curves in Figures 2.5(a) and 2.5(b) which are very similar because the waiting time was

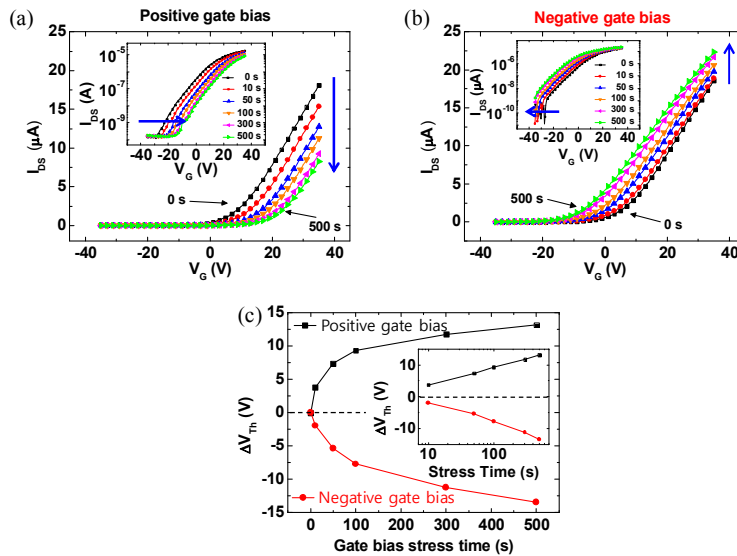


Figure 2.5 (a, b) I_{DS} - V_G curves measured in ambient conditions after (a) +35 V and (b) -35 V gate bias stress was applied for different stress duration times. (c) The shift in the threshold voltage (ΔV_{Th}) for each measurement with respect to the value for the initial curve (“0 s” curve). The inset is the plot made on the logarithmic scale of stress time.

sufficient for the device to fully recover. From Figure 2.5(a), one can see that under a positive gate bias stress, the current decreased and the threshold voltage shifted in the positive gate bias direction.

We repeated the gate bias stress measurements with a negative gate bias. Figure 2.5(b) displays the transfer characteristics data obtained after we applied a constant -35 V gate bias for different times while all the other conditions were the same as in Figure 2.5(a). For the negative gate bias stress (Figure 2.5(b)), the current increased and the threshold voltage shifted in the negative gate bias direction. The results in Figure 2.5 are consistent with the observed results in Figure 2.4: a positive (negative) gate bias stress decreased (increased) the current and the threshold voltage shifted in the positive (negative) gate bias direction. These observations are due to the charge trapping associated with ambient effect. The shift in the threshold voltages at each measurement as a function of the gate bias stress time for both the positive and negative gate biases was plotted in Figure 2.5(c). The inset in Figure 2.5(c) is the logarithm time scale. One can see that the shift in the threshold voltage increased with respect to the value for initial curve (0 sec) as the gate bias stress time increased for both gate bias polarities. When the gate bias is applied for long enough, the absorbed oxygen and/or water will be saturated and the shift in the threshold voltage will also be saturated.

2.3.4 Gate voltage sweep rate, sweep range dependence

We also examined the effect of the gate bias sweep rate on the device's characteristics. Figure 2.6(a) shows the transfer characteristics measured at ambient conditions with a gate bias sweep from +35 V to -35 V at different sweep rates (from a fast rate of 8 V/s to a slow rate of 0.1 V/s). As shown in Figure 2.6(a), as the sweep rate

decreased, the current decreased, and the threshold voltage shifted in the positive gate bias direction. The positive shift of the threshold voltage as the sweep rate decreased can be observed in the logarithmic-scale (Figure 2.6(b)) and linear-scale plot (Figure 2.6(b) inset). This behavior is consistent with the data in Figures 2.4(a) and 2.5(a) because a slow sweep rate means a longer gate bias stress time. Similar behavior was observed in the case of the opposite gate bias sweep direction (*i.e.*, the sweep from -35 V to +35 V with the same sweep rate conditions), as shown in Figures 2.6(c) and 2.6(d).

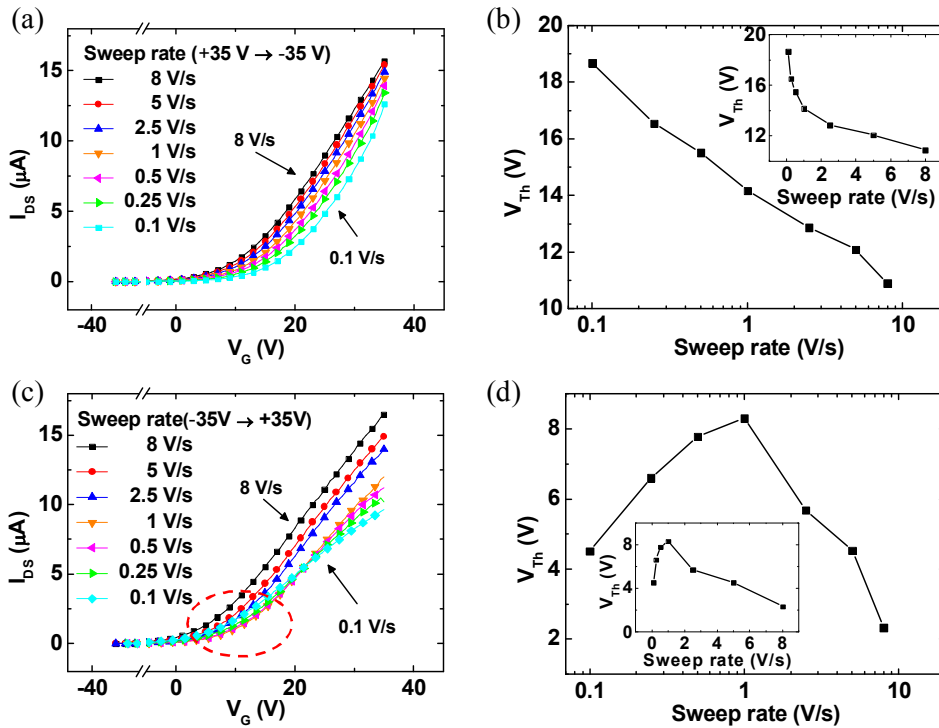


Figure 2.6 (a, c) I_{DS} - V_G curves measured in ambient conditions with different gate bias sweep rates ranging from 8 V/s to 0.1 V/s. The gate bias was swept (a) from +35 V to -35 V and (c) from -35 V to +35 V. (b, d) The threshold voltage (V_{Th}) at each measurement for different sweep rates for gate bias swept (b) from +35 V to -35 V and (d) from -35 V to +35 V. Insets in (b, d) are plots made as the linear scale of sweep rate.

As sweep rate decreased, the current also decreased, and the threshold voltage shifted in the positive gate bias direction as a result of the longer stress time of the positive gate bias at the slower sweep rates. However, at the slower sweep rates of 0.5, 0.25, and 0.1 V/s, the current first increased around a low gate bias (circled in Figure 2.6(c)), then it decreased at larger positive gate bias. This can be explained by considering the positive and negative gate bias sweep ranges separately; at slower rates, when the gate bias was swept from -35 V to 0 V, the current tended to increase first (consistent with the case of Figures 2.4(b) and 2.5(b)), and then when the gate bias was continuously swept from 0 V to +35 V, the current decreased (consistent with the case of Figures 2.4(a) and 2.5(a)). This phenomenon resulted in an increase and then decrease in the threshold

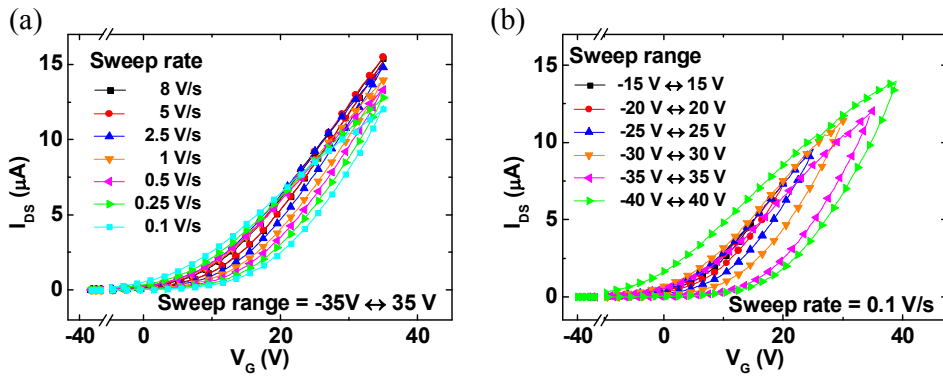


Figure 2.7 (a) The hysteresis I_{DS} - V_G curves of double sweep (from -35 V to +35 V and then back to -35 V) at different gate bias sweep rates measured in the ambient environment. (b) The hysteresis I_{DS} - V_G curves with different gate bias sweep range at a fixed gate bias sweep rate of 0.1 V/s in ambient.

voltage as the sweep rate slowed (from 8 V/s to 0.1 V/s), as shown in Figure 2.6(d).

Figure 2.7 displays the effect of gate bias double sweeps, *i.e.*, -35 V to +35 V and then back to -35 V, at the same sweep rates. The results are shown in Figure 2.7(a). As the sweep rate decreased, the current tended to increase in the negative gate bias range (-35 V to 0 V) and to decrease during the positive gate bias range (0 V to +35 V); thus, there is a hysteresis in the double sweep loop. This hysteresis effect became more obvious at the slower sweep rates because the slower sweep rates (*i.e.*, longer gate bias time) enhanced the gate bias stress effects. Similarly, this hysteresis effect became more significant as the gate bias sweep range increased (Figure 2.6(b)).

2.3.5 Environmental condition dependence

To investigate the ambient effect, we repeated the gate bias stress measurements in a vacuum (5.6×10^{-5} torr). Figure 2.8(a) shows the transfer characteristic curves that were measured in a vacuum with the same measurement conditions as the data in Figure 2.5(b). Figure 2.8(b) shows the data measured in vacuum at the same conditions as the data in Figure 2.6(a). No significant gate bias stress effects were observed in the vacuum environment. There were small shifts observed in the data, especially in Figure 2.8(a). These shifts are due to the interfacial traps at the interface between the MoS₂ and SiO₂ dielectric layer in response to the gate bias stress.

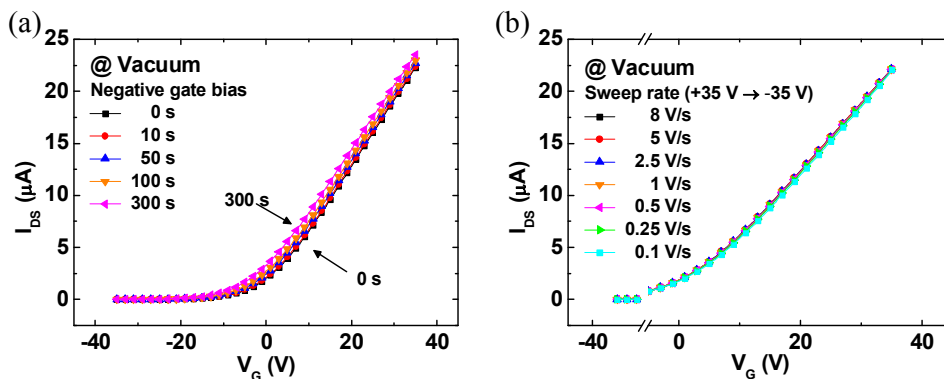


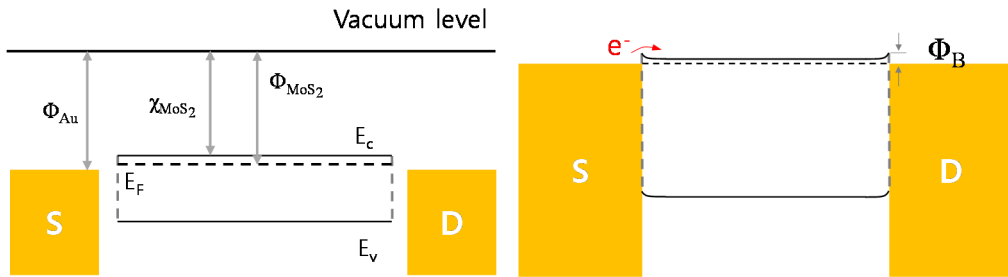
Figure 2.8 (a) I_{DS} - V_G curves measured in vacuum after -35 V gate bias stress was applied for different stress duration time. (b) I_{DS} - V_G curves measured in vacuum during the gate bias sweep from +35 V to -35 V with different gate bias sweep rates.

2.3.6 Energy band schematic

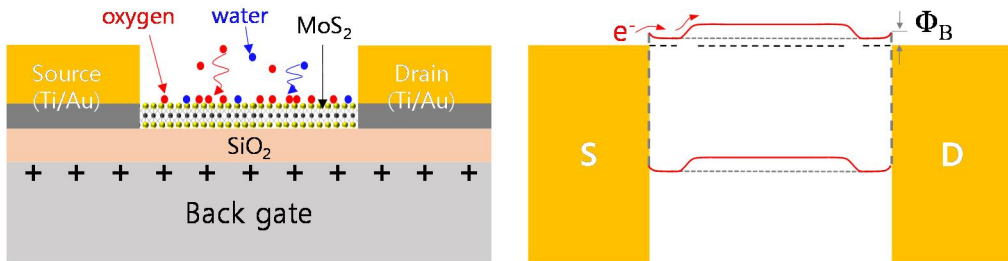
Next, we discuss the gate bias stress effect on the MoS₂ FET using energy band diagram schematics. Figure 2.9 shows the energy band diagram for $V_{SD} = 0$ V and $V_G = 0$ V at ambient conditions for three cases: no gate bias stress, positive gate bias stress, and negative gate bias stress. To understand the charge transport, we need to consider the metal/MoS₂ contact interfaces at the source and drain electrodes because metal contacts to semiconducting MoS₂ can create Schottky barriers, which can dominate the electronic properties of MoS₂-based devices. We first assume that although a bandgap of MoS₂ is dependent on their thickness, our MoS₂ nanoflakes have a bandgap of about 1.2 eV similar to that of the bulk. In addition, MoS₂ has an electron affinity of 4.0 eV,[37,38] a work function of 4.6-4.9 eV.[39,40] Contact metals used as source and drain electrodes in our study are Ti and Au in which their work functions are 3.9–4.3 eV and 5.1–5.4 eV, respectively. Because the Ti layer is an adhesion layer for Au contact to a MoS₂ nanoflake, we considered the band alignment of Au-MoS₂ interfaces at the source and drain. According to Popov *et al.*,[41] the Ti can play a role in modifying the interface properties due to an increase in the density of state at the Fermi level (E_F), resulting in a low-resistance Ohmic contact. Our results clearly indicate that the MoS₂ FET device exhibit the typical n-type semiconducting behavior with low-resistance Ohmic contact at low voltages in the output curves (see $I_{DS}-V_{DS}$, the inset of Figure 2.3(b)), which is consistent with previous results.[38,39,42] Accordingly, we can consider the band alignment for the Au/MoS₂ contacts at the source and drain with a very small Schottky barrier (Φ_B), as shown in Figure 2.9(a). Here, we assume that the gate bias stress effects can be due to the adsorption/desorption of oxygen and water on the MoS₂ surface and the MoS₂ region underneath metal contact is not affected by such adsorption/desorption. In the case of the

application of identical positive gate bias stress, the accumulated electron density in channel region increases by positive electric field and the resulting adsorbed oxygen and water concentration on the MoS₂ channel surface is also increased in which the adsorbed oxygen and water can capture charge carriers from the conduction band in MoS₂ channel.

(a) No gate bias stress



(b) Positive gate bias stress (oxygen and water adsorption)



(c) Negative gate bias stress (oxygen and water desorption)

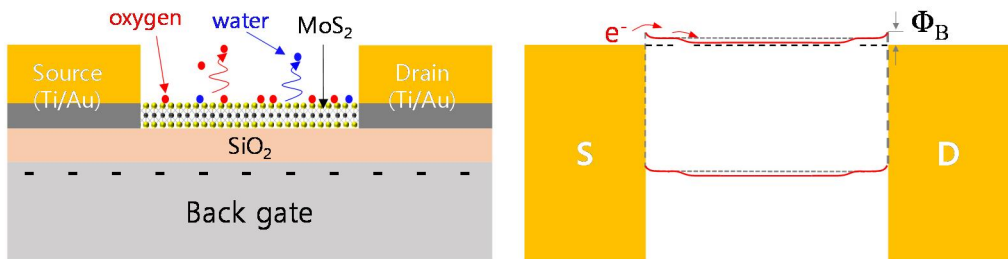


Figure 2.9 The schematics of the energy band diagram at $V_G = 0$ V in the ambient environment when (a) no gate bias stress, (b) positive gate bias stress, and (c) negative gate bias stress is applied.

This causes channel depletion and the observed positive V_{th} shift (Figures 2.4(a) and 2.5(a)). As shown in Figure 2.9(b), carriers first travel through the interface region between the MoS₂ and metal contact, and then traverse the channel depletion-induced conduction barrier before entering into the MoS₂ channel. In contrast, when a negative gate bias stress is applied, oxygen and water desorb in response to the identical negative gate electric field. The electrons that are trapped by the adsorbed oxygen and water at the MoS₂ channel region are released and transferred to the MoS₂ channel by the application of negative gate bias stress, which results in a reduction of the carrier depletion of the MoS₂ FET. As shown in Figure 2.9(c), the desorption of oxygen and water causes the accumulation of charge carriers from the conduction band in MoS₂ channel, lead to the observed negative V_{th} shift (Figure 2.4(b) and 2.5(b)). These results suggest that the passivation of the MoS₂ surface will be important to obtain reproducible results and to minimize the ambient effect.

2.4. Conclusion

We investigated the electrical-stress-induced threshold voltage instability of multi-layered MoS₂ FET devices with a back-gated configuration under an ambient environment. When a positive (negative) gate bias stress was applied to the device, the current decreased (increased) and the threshold shifted in the positive (negative) gate bias direction. This effect was enhanced when a longer gate bias time or a slower sweep rate of the gate bias was applied. These gate bias stress effects can be explained by the charge trapping mainly due to the adsorption (desorption) of oxygen and/or water on the MoS₂ surface with a positive (negative) gate bias under ambient conditions. Our study has

important implications for a better design of functional nanodevices based on two-dimensional layered calcogenides for wide nanoelectronic device applications.

References

- [1] Novoselov, K.; Geim, A. K.; Morozov, S.; Jiang, D.; Zhang, Y.; Dubonos, S.; Grigorieva, I.; Firsov, A. *Science* **2004**, *306*, 666-669.
- [2] Novoselov, K. S.; Jiang, D.; Schedin, F.; Booth, T. J.; Khotkevich, V. V.; Morozov, S. V.; Geim, A. K. *P. Natl. Acad. Sci. U.S.A.* **2005**, *102*, 10451-10453.
- [3] Li, X.; Wang, X.; Zhang, L.; Lee, S.; Dai, H. *Science* **2008**, *319*, 1229-1232.
- [4] Radisavljevic, B.; Radenovic, A.; Brivio, J.; Giacometti, V.; Kis, A. *Nat. Nanotechnol.* **2011**, *6*, 147-150.
- [5] Kam, K.; Parkinson, B. *J. Phys. Chem.* **1982**, *86*, 463-467.
- [6] Mak, K. F.; Lee, C.; Hone, J.; Shan, J.; Heinz, T. F. *Phys. Rev. Lett.* **2010**, *105*, 136805.
- [7] Bertolazzi, S.; Brivio, J.; Kis, A., *ACS Nano* **2011**, *5*, 9703-9709.
- [8] Castellanos-Gomez, A.; Poot, M.; Steele, G. A.; van der Zant, H. S.; Agrait, N.; Rubio-Bollinger, G. *Adv. Mater.* **2012**, *24*, 772-775.
- [9] Eda, G.; Yamaguchi, H.; Voiry, D.; Fujita, T.; Chen, M.; Chhowalla, M. *Nano Lett.* **2011**, *11*, 5111-5116.
- [10] Scalise, E.; Houssa, M.; Pourtois, G.; Afanas'ev, V.; Stesmans, A. *Nano Res.* **2012**, *5*, 43-48.
- [11] Perkins, F. K.; Friedman, A. L.; Cobas, E.; Campbell, P. M.; Jernigan, G. G.; Jonker, B. T. *Nano Lett.* **2013**, *13*, 668-673.
- [12] Lee, H. S.; Min, S. W.; Park, M. K.; Lee, Y. T.; Jeon, P. J.; Kim, J. H.; Ryu, S.; Im, S. *Small* **2012**, *8*, 3111-3115.
- [13] Wang, H.; Yu, L.; Lee, Y. H.; Shi, Y.; Hsu, A.; Chin, M. L.; Li, L. J.; Dubey, M.; Kong, J.; Palacios, T. *Nano. Lett.* **2012**, *12*, 4674-4680.
- [14] Yin, Z.; Zeng, Z.; Liu, J.; He, Q.; Chen, P.; Zhang, H. Memory Devices Using a Mixture of MoS₂ and Graphene Oxide as the Active Layer. *Small* **2013**, *9*, 727-731.
- [15] Radisavljevic, B.; Whitwick, M. B.; Kis, A. *ACS Nano* **2011**, *5*, 9934-9938.
- [16] Choi, W.; Cho, M. Y.; Konar, A.; Lee, J. H.; Cha, G. B.; Hong, S. C.; Kim, S.; Kim, J.; Jena, D.; Joo, J. *et al. Adv. Mater.* **2012**, *24*, 5832-5836.
- [17] Li, H.; Yin, Z.; He, Q.; Li, H.; Huang, X.; Lu, G.; Fam, D. W. H.; Tok, A. I. Y.; Zhang, Q.; Zhang, H. *Small* **2012**, *8*, 63-67.

- [18] Kim, S.; Konar, A.; Hwang, W. S.; Lee, J. H.; Lee, J.; Yang, J.; Jung, C.; Kim, H.; Yoo, J. B.; Choi, J. Y. *et al.* **2012**, *3*, 1011.
- [19] Park, W.; Park, J.; Jang, J.; Lee, H.; Jeong, H.; Cho, K.; Hong, S.; Lee, T. *Nanotechnology* **2013**, *24*, 095202.
- [20] Davis, S. M.; Carver, J. C. *Appl. Surf. Sci.* **1984**, *20*, 193-198.
- [21] Late, D. J.; Liu, B.; Matte, H. S. S. R.; Dravid, V. P.; Rao, C. N. R. *ACS Nano* **2012**, *6*, 5635-5641.
- [22] Qiu, H.; Pan, L.; Yao, Z.; Li, J.; Shi, Y.; Wang, X. *Appl. Phys. Lett.* **2012**, *100*, 123104.
- [23] Pierret, R. F. *Semiconductor Device Fundamentals*. Addison Wesley, 1996.
- [24] Yoon, Y.; Ganapathi, K.; Salahuddin, S. *Nano Lett.* **2011**, *11*, 3768-3773.
- [25] Liu, H.; Neal, A. T.; Ye, P. D. *ACS Nano* **2012**, *6*, 8563-8569.
- [26] N, Arora. *MOSFET models for VLSI Circuit simulation: Theory and Practice*. Springer 1993.
- [27] Maeng, J.; Jo, G.; Kwon, S.-S.; Song, S.; Seo, J.; Kang, S.-J.; Kim, D.-Y.; Lee, T. *Appl. Phys. Lett.* **2008**, *92*, 233120.
- [28] Choe, M.; Park, W.; Kang, J. W.; Jeong, S.; Hong, W. K.; Lee, B. H.; Park, S. J.; Lee, T. *Nanotechnology* **2012**, *23*, 485201.
- [29] Jeong, J. K.; Won Yang, H.; Jeong, J. H.; Mo, Y.-G.; Kim, H. D. *Appl. Phys. Lett.* **2008**, *93*, 123508.
- [30] Suresh, A.; Muth, J. F. *Appl. Phys. Lett.* **2008**, *92*, 033502.
- [31] Lee, J.-M.; Cho, I.-T.; Lee, J.-H.; Kwon, H.-I. *Appl. Phys. Lett.* **2008**, *93*, 093504.
- [32] Chang, E.; Cibuzar, G.; Pande, K. *IEEE T. Electron Dev.* **1988**, *35*, 1412-1418.
- [33] Sato, Y.; Takai, K.; Enoki, T.; *Nano. Lett.*, **2011**, *11*, 3468-3475.
- [34] Powell, M. J.; *IEEE T. Electron Dev.* **1989**, *36*, 2753-2763.
- [35] Jahinuzzaman, S. M.; Sultana, A.; Sakariya, K.; Servati, P.; Nathan, A.; *Appl. Phys. Lett.* **2005**, *87*, 023502.
- [36] Lelis, A. J.; Habersat, D.; Green, R.; Ogunniyi, A.; Gurfinkel, M.; Suehle, J.; Goldsman, N.; *IEEE T. Electron Dev.* **2008**, *55*, 1835-1840.
- [37] Han, S. W.; Kwon, H.; Kim, S. K.; Ryu, S.; Yun, W. S.; Kim, D. H.; Hwang, J. H.; Kang, J.-S.; Baik, J.; Shin, H. J. *et al. Phys. Rev. B* **2011**, *84*, 045409.

- [38] Das, S.; Chen, H.-Y.; Penumatcha, A. V.; Appenzeller J. *Nano Lett.* **2013**, 13, 100–105.
- [39] Liu, K.-K.; Zhang, W.; Lee, Y.-H.; Lin, Y.-C.; Chang, M.-T.; Su, C. -Y.; Chang, C. -S.; Li, H.; Shi, Y.; Zhang, H. *et al. Nano Lett.* **2012**, 12, 1538–1544.
- [40] Giridharagopal, R.; Kelly, K. F. *ACS Nano* **2008**, 2, 1571-1580.
- [41] Popov, I.; Seifert, G.; *Phys. Rev. Lett.* **2012**, 108, 156802.
- [42] Ghatak, S.; Pal, A. N.; Ghosh, *ACS Nano* **2011**, 5, 7707-7712.

Chapter 3. Electrical Properties of MoS₂ FETs with Thiol

Molecule Surface Treatment

In this chapter, we will discuss about the electrical optical characteristics of thiol treated MoS₂ FETs. We investigated the physical properties of molybdenum disulfide atomic crystals with a sulfur vacancy passivation after treatment with alkanethiol molecules including their electrical, Raman, and photoluminescence (PL) characteristics. MoS₂, one of the transition metal dichalcogenide materials, is a promising two-dimensional semiconductor material with good physical properties. It is known that sulfur vacancies exist in MoS₂, resulting in the n-type behavior of MoS₂. The sulfur vacancies on the MoS₂ surface tend to form covalent bonds with sulfur containing groups. In this study, we deposited alkanethiol molecules on MoS₂ field effect transistors and then characterized the electrical properties of the devices before and after the alkanethiol treatment. We observed that the electrical characteristics of MoS₂ FETs dramatically changed after the alkanethiol treatment. We also observed that the Raman and PL spectra of MoS₂ films changed after the alkanethiol treatment. These effects are attributed to the thiol (-SH) end groups in alkanethiols bonding at sulfur vacancy sites, thus altering the physical properties of the MoS₂. This study will help us better understand the electrical and optical properties of MoS₂ and suggest a way of tailoring the properties of MoS₂ by passivating sulfur vacancy with thiol molecules.

3.1. Introduction

Recently, transition metal dichalcogenide (TMD) two-dimensional (2D) atomic layered materials have drawn considerable attention as promising semiconductors for future ultrathin layered nanoelectronic device applications.[1,2] Although graphene has several favorable features for use as a 2D layered material, such as high carrier mobility, transparency and good mechanical properties, graphene has an obvious limitation for use

as a semiconductor active channel because of the absence of an energy band gap.[3-5] Unlike graphene, TMD materials have a semiconductor band gap with advantages, such as availability of complex device structures with semiconductor properties, good flexibility, and high transparency.[6,7] Molybdenum disulfide, a member of the TMD family, has been widely studied due to these advantages. MoS₂ is known to have a direct band gap of ~1.9 eV as a single MoS₂ layer and an indirect band gap of ~1.2 eV as a bulk MoS₂ crystal.[8,9] Single-layer MoS₂ also has a good carrier mobility (~tens of cm²/Vs or more) and a high current on/off ratio (~10⁵ or more).[10-18] Like graphene, MoS₂ flakes with a thickness of a single layer or multiple layers can be prepared by a mechanical exfoliation method using Scotch Tape due to a weak van der Waals interaction between MoS₂ layers.[6] Additionally, large area MoS₂ films can be synthesized by chemical vapor deposition or by other methods.[19-21]

One of the potential candidate is the sulfur vacancies of MoS₂. [22,23] MoS₂ has sulfur vacancies that are considered as cause of n-type behavior of MoS₂. [22] The sulfur vacancy sites, unsaturated Mo on the surface of MoS₂, have a tendency to covalently bond with sulfur containing groups. [24-26] Because of this, MoS₂ has been used as a dehydrosulfurization catalyst, *i.e.*, the sulfur vacancies on the basal plane of MoS₂ act as catalytic reaction sites. [24-26] Therefore, molecules with thiol (-SH) functional groups will form a chemisorbed bond with MoS₂ at the sulfur vacancy positions. Makarova *et al.* have examined the adsorption of thiol molecules with scanning tunneling microscopy, and they indeed observed selective adsorption of thiol molecules at sulfur vacancies on the basal plane of MoS₂. [24] If the sulfur vacancies are important for the n-type characteristics of MoS₂ when it is used as a semiconductor device, then the treatment of

thiol molecules on MoS₂ would be able to alter the electrical properties of MoS₂ by passivating sulfur vacancies of MoS₂ with thiol molecules.

In this study, we have investigated how the adsorption of thiol molecules on MoS₂ influences the physical and electrical properties of MoS₂. For this purpose, we deposited alkanethiol (HS(CH₂)_{n-1}CH₃) molecules on MoS₂ surfaces. Alkanethiols are one of the most widely studied thiol molecules in molecular-based electronic devices.[27-32] We studied and compared the electrical characteristics of field effect transistors made with exfoliated MoS₂ flakes prior to and after alkanethiol treatment. We also studied and systematically compared the Raman and photoluminescence spectra of exfoliated MoS₂ flakes prior to and after treatment with alkanethiols.

3.2. Experiments

3.2.1. Device fabrication process

Figure 3.1 explains the device fabrication procedure. First, we prepared 270-nm-thick SiO₂ on highly p++ doped Si (resistivity $\sim 5 \times 10^{-3} \Omega \text{ cm}$) substrate that can be used as back gate. Next, the MoS₂ flakes were exfoliated from a bulk MoS₂ crystal (SPI supplier, USA) by micromechanical exfoliation method. After we transferred the MoS₂ flakes on the device substrate, we used an optical microscope to find proper MoS₂ flakes which can be made to MoS₂ field effect transistors. After finding proper MoS₂ flakes, we measured the height of the MoS₂ flake using atomic force microscopy (AFM). Then, we spin-coated MMA (8.5) MMA (9% concentration in ethyl lactate) with 4000 rpm for 50 sec. And we baked the sample at 180°C for 1 minute and 30 sec. Next, the PMMA 950K (5% concentration in anisole) was spin-coated with 4000 rpm for 50 sec. And the samples were baked with 180°C for 1 minute and 30 sec. The source-drain electrodes patterns

were made by using an electron beam lithography (JSM-6510, JEOL). The pattern development was done with MIBK:IPA (1:3) solution for development time of 50 sec. After development, we deposited Ti (50-nm-thick) as the source and drain electrodes by using an electron beam evaporator.

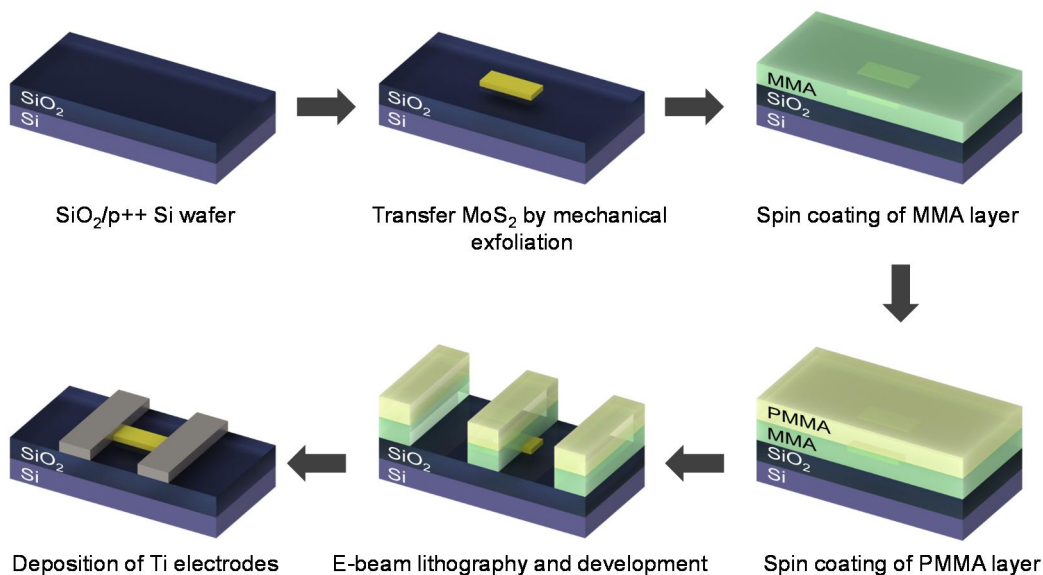


Figure 3.11 Schematics illustrating the device fabrication procedures.

3.2.2. Thiol molecule treatment

After electrical characterization of the MoS₂ FET devices, we deposited hexadecanethiol (HS(CH₂)₁₅CH₃) on the MoS₂ FET devices. For this purpose, we dipped the MoS₂ FET devices in 5 mM hexadecanethiol in ethanol solution for 15 hours in a N₂-filled glove box. Then, we rinsed the devices with ethanol and measured the electrical properties of the hexadecanethiol-treated MoS₂ FET devices, again under vacuum conditions.

3.3. Results & Discussions

3.3.1. Electrical properties of MoS₂ FETs

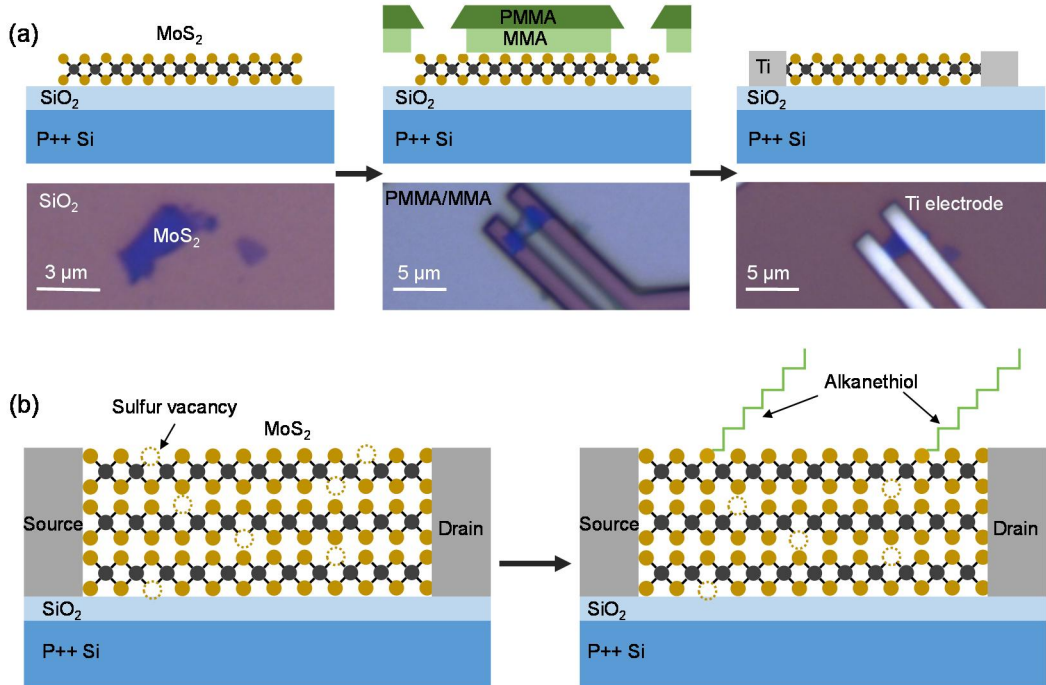


Figure 3.12 (a) Schematic images of the fabrication process of MoS₂ FETs with the optical images shown under the each schematic image. (b) Schematic images of a MoS₂ FET before (left) and after (right) the alkanethiol molecule treatment.

Figure 3.2(a) illustrates the fabrication process for MoS₂ FET devices. The upper and lower figures in Figure 3.2(a) show the schematics and optical microscopic images of a sample during fabrication of the device. First, we prepared the MoS₂ flakes by micromechanical exfoliation from a bulk MoS₂ crystal. The exfoliated MoS₂ flakes were transferred to a 270 nm thick SiO₂ layer on a heavily doped p++ Si substrate, which can be used as a back gate in FET devices (Figure 3.2(a) left). We found appropriate flakes of transferred MoS₂ that can be used for fabrication of FET devices using an optical microscope, and we measured the height of the MoS₂ flakes using an atomic force

microscope (AFM). Next, we used an electron beam lithography system to make the source and drain electrode patterns of the FET devices. Here, to prepare well-defined electrode patterns, we used double layers of resists; an electron resist polymer and a buffer layer polymer (Figure 3.2(a) middle). Then, 50-nm thick Ti was deposited as the source and drain electrodes using an electron beam evaporator (Figure 3.2(a) right).

After we fabricated MoS₂ flake devices, we deposited alkanethiol molecules on the fabricated devices. As explained previously, the thiol molecules tend to form a chemisorbed bond with MoS₂ at the sulfur vacancy positions. Figure 3.2(b) shows the schematic images of a MoS₂ FET device before and after the alkanethiol treatment. We placed MoS₂ FET devices in the alkanethiol solution for 15 hours to allow alkanethiol molecules to be adsorbed on the MoS₂ surface. We characterized and compared the electrical properties of the fabricated MoS₂ FET devices before and after the alkanethiol treatment to examine the effect of alkanethiol absorption on the MoS₂ FET devices. The electrical characterization was performed using a semiconductor parameter analyzer in a probe station. We also systematically characterized some of the transferred MoS₂ flakes (not a FET device structure) on SiO₂/Si substrates prior to and after the alkanethiol treatment process with Raman spectroscopy and photoluminescence. Note that in the study of MoS₂ FET devices, we did not use Au as the electrode because alkanethiol molecules can form a self-assembled monolayer (SAM) on a Au surface. Furthermore, SAM-modified Au electrodes may change the Fermi level of the electrodes and thus cause unwanted source-drain current changes, which may complicate the analysis.

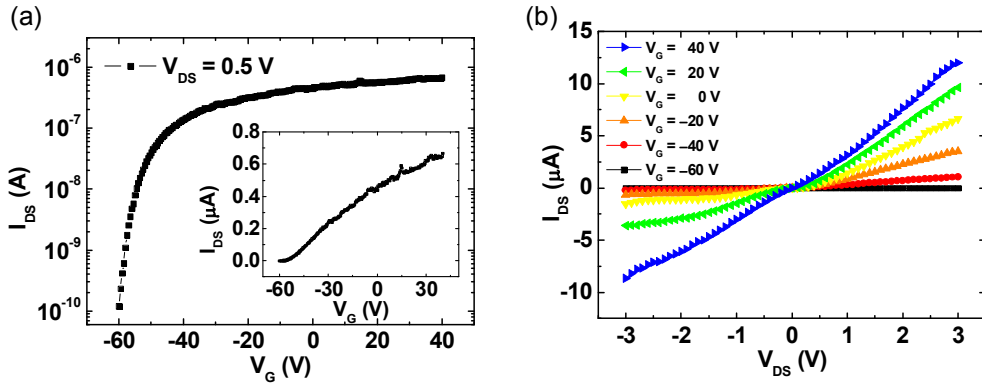


Figure 3.13 (a) I_{DS} - V_G curve measured at a fixed $V_{DS} = 0.5$ V with logarithmic scale. The inset shows I_{DS} - V_G curves with linear scale. (b) I_{DS} - V_{DS} curves measured with V_G varying from 40 to -60 V.

We first measured the basic electrical characteristics of the MoS₂ FET devices prior to the alkanethiol treatment. Figure 3.3(a) shows the transfer curve (source-drain current *versus* gate voltage, I_{DS} - V_G) of a MoS₂ FET device measured at a fixed source-drain voltage ($V_{DS} = 0.5$ V) on a logarithmic scale for the source-drain current. The same transfer curve is plotted on the linear scale for the current in the inset of Figure 3.3(a). Figure 3.3(b) displays the output curves (source-drain current *versus* source-drain voltage, I_{DS} - V_{DS}) of the device measured with gate voltages varying from 40 to -60 V with a step of 20 V. All of the electrical data were measured in a vacuum ($\sim 10^{-4}$ torr) to avoid unwanted effects from the ambient environment, such as those from water and oxygen. MoS₂ FET devices may suffer from environmental effects.[33,34] One thing to notice in Figure 3.3 is that there was no obvious off-state observed. This can be explained by thermally assisted tunneling through thin Schottky barrier at Ti/MoS₂ contact.[35] The Ti metal has a work function of ~ 4.3 eV and MoS₂ has a work function in the range of 4.6–4.9 eV. However, although the work function of Ti is smaller than that of MoS₂,

there is a Schottky barrier formed between the Ti and MoS₂. [39-41] When the Schottky barrier is low and its thickness is ultrathin as in the case of Ti/MoS₂, the charges can transport *via* thermionic emission and thermally assisted tunneling conduction mechanisms. [35] And this is the reason of absence of obvious off-state in MoS₂ with Ti contacts at room temperature.

We estimated the mobility using the following formula, $\mu = \left[\frac{dI_{DS}}{dV_G} \right] \times [L / (WC_i V_{DS})]$. In this formula, W is the channel width, L is the channel length, and $C_i = \frac{\epsilon_0 \epsilon_r}{d} \cong 1.3 \times 10^{-4} \text{ F/m}^2$ is the capacitance between the MoS₂ channel and the p++ Si layer per unit area, where ϵ_r is the dielectric constant of SiO₂ (~3.9), ϵ_0 is the vacuum permittivity, and d is the thickness of the SiO₂ layer (270 nm). In this study, we fabricated and characterized a total of ten MoS₂ FET devices that were prepared from mechanically exfoliated MoS₂ flakes and electron beam lithography. The thickness of exfoliated MoS₂ flakes was found to be in a range from 2.1 to 10.9 nm from AFM, which corresponds to a MoS₂ layer number of 3-17 layers. The estimated mobility values of the MoS₂ FET devices fabricated in this study were found to be in a range from 2.5 to 35.2 cm²/Vs. Additionally, we calculated the carrier concentration of the MoS₂ FETs using the following formula, $n_e = Q/e = C_G |V_G - V_{Th}| / e$, where C_G is the capacitance of the SiO₂ dielectric layer, $e = 1.6 \times 10^{-19}$, C is the elementary charge and V_{Th} is the threshold voltage of the FET devices. The mobility and carrier concentrations were measured using the same condition of $V_G = 20 \text{ V}$ and $V_{DS} = 0.5 \text{ V}$. We determined the V_{Th} values as the x-axis intercept from a linear fitting of the transfer curves. Then, the carrier concentration of the MoS₂ FET devices were found to be in a range from $2.4 \times 10^{12} \text{ cm}^{-2}$ to $7.1 \times 10^{12} \text{ cm}^{-2}$.

3.3.2. Electrical properties of MoS₂ FETs with Thiol molecule treatment

Figure 3.4(a) shows the transfer characteristic curves on a logarithmic scale for a MoS₂ FET device. The data represented with filled and open circular symbols are the transfer curves measured before (labelled with “Pristine”) and after the hexadecanethiol treatment, respectively. The inset of Figure 3(a) is the transfer characteristic curves on a linear current scale. The source-drain current level dramatically decreased by ~45%; from 0.58 μA (prior to the molecular treatment) to 0.32 μA (after the molecular treatment) measured at $V_G = 20\text{ V}$ and $V_{DS} = 0.5\text{ V}$. The current decrease can be observed in the

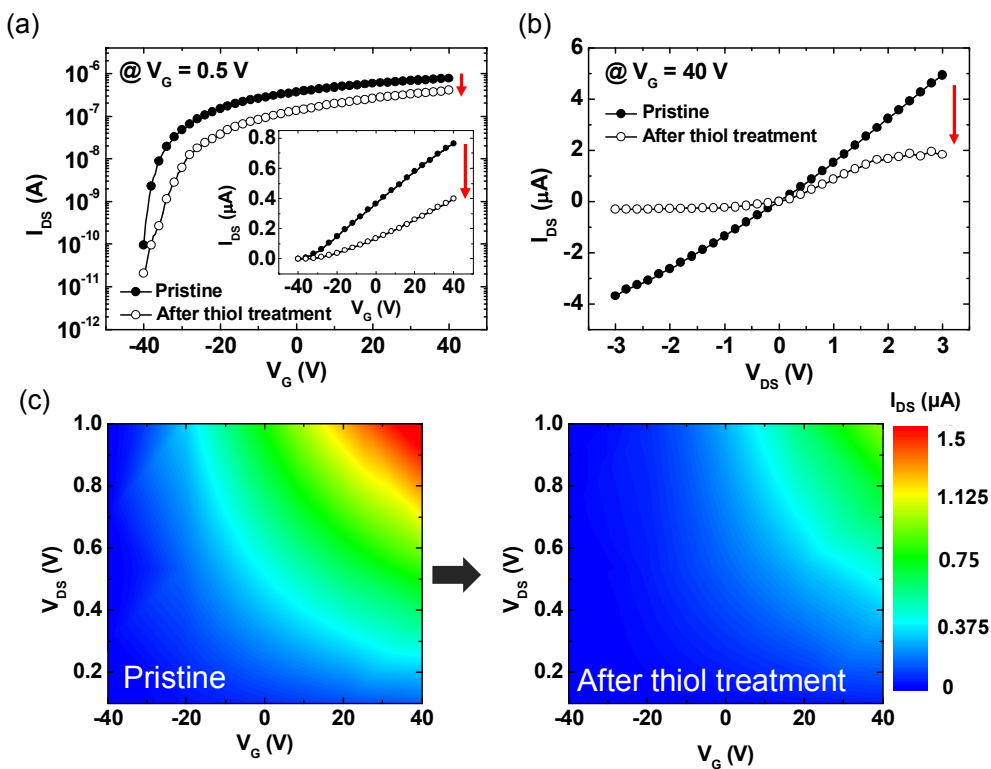


Figure 3.14 (a) I_{DS} - V_G curves measured before and after the hexadecanethiol treatment with logarithmic scale. The inset shows I_{DS} - V_G curves with linear scale. (b) I_{DS} - V_{DS} curves measured before and after the hexadecanethiol treatment. (c) The contour plots of I_{DS} as a function of V_G and V_{DS} before (left) and after (right) the hexadecanethiol treatment.

output characteristic curves, as shown in Figure 3.4(b).

This phenomenon can be more clearly observed in contour plots of the current. Figure 3.4(c) displays the contour plots of the source-drain current as a function of V_G and V_{DS} for the MoS₂ FET device that were obtained from the transfer characteristics curves measured for V_{DS} in the range of 0.1 to 1 V, and V_G in the range of -40 to 40 V before and after the hexadecanethiol treatment. Here, one can clearly notice that the channel current in the device decreased after the molecular treatment.

The observation of the current decrease phenomenon in MoS₂ FETs after the alkanethiol treatment can be explained in the following manner. Thiol molecules have a sulfur atom at the end group and the sulfur-containing groups have a tendency to form covalent bonds with unsaturated Mo edges of vacancy defects on the surface of MoS₂. [24-26] In the vacancy defect sites there are free electrons in unsaturated Mo atoms which do not belong to any chemical bond, and these electrons can behave as charge carriers. However, after the thiol molecule treatment, the thiol molecules are chemically absorbed at the sulfur vacancy sites on the surface of MoS₂, which decreases the number of free electrons in MoS₂. Also, note that the adsorbed alkanethiol molecules or possible solution residue may behave as defects such as scattering centers, which can also cause additional effect as the current decrease after the molecule treatment. The density of sulfur vacancy has been estimated on the order of 10^{13} cm⁻² from aberration-corrected transmission electron microscopy (TEM) images. [22] It is desired to investigate to estimate the percentage of sulfur vacancy that are occupied by alkanethiol molecules after the molecule treatment using atomic resolution TEM or other analyses, which is unfortunately beyond the scope of our study.

We consistently observed similar current decrease phenomena with other MoS₂ FET devices in response to the alkanethiol treatment, and the current contour plots for other MoS₂ FET devices before and after the treatments. To confirm that the reason for the current decrease in the devices is indeed due to the effect of the adsorbed alkanethiol molecules, we treated MoS₂ FET devices in the same way that we processed alkanethiol-treated MoS₂ FET devices but in an ethanol solution that did not contain any alkanethiol molecules. In this case, the source-drain current of the ethanol-treated MoS₂ FET device did not decrease significantly compared with the case prior to the ethanol treatment. Also notice that the decreased current of alkanethiol-treated MoS₂ FETs recovered the channel current to the value of pristine condition when we annealed the devices at elevated temperature over 473 K.

The current reduction after the thiol molecule treatment can be due to the molecules acting as trap sites, or the molecules passivating sulfur vacancies and decreasing the carrier concentration. To find out the dominant mechanism among these, we performed temperature-variable I-V measurements for the devices before and after the alkanethiol molecule treatment. We first measured the V_G - I_{DS} curves of the MoS₂ FET device in the temperature range from 80 to 320 K as shown in the left part of Figure 3.5(a). And then, we treated alkanethiol molecules to the device and measured again, as the results are shown in the right part of Figure 3.5(a). From Figure 3.5(a), we can notice that the current level of the device decreased and the threshold voltage shifted to the positive gate voltage direction while the subthreshold swing (SS) value did not change significantly. Figure 3.5(b) shows the carrier concentration (black symbols) and threshold voltage (blue symbols) of the device before and after the molecule treatment. Filled and empty square symbols in this figure represent the data which were measured before and

after the molecule treatment, respectively. The carrier concentration was estimated at V_G

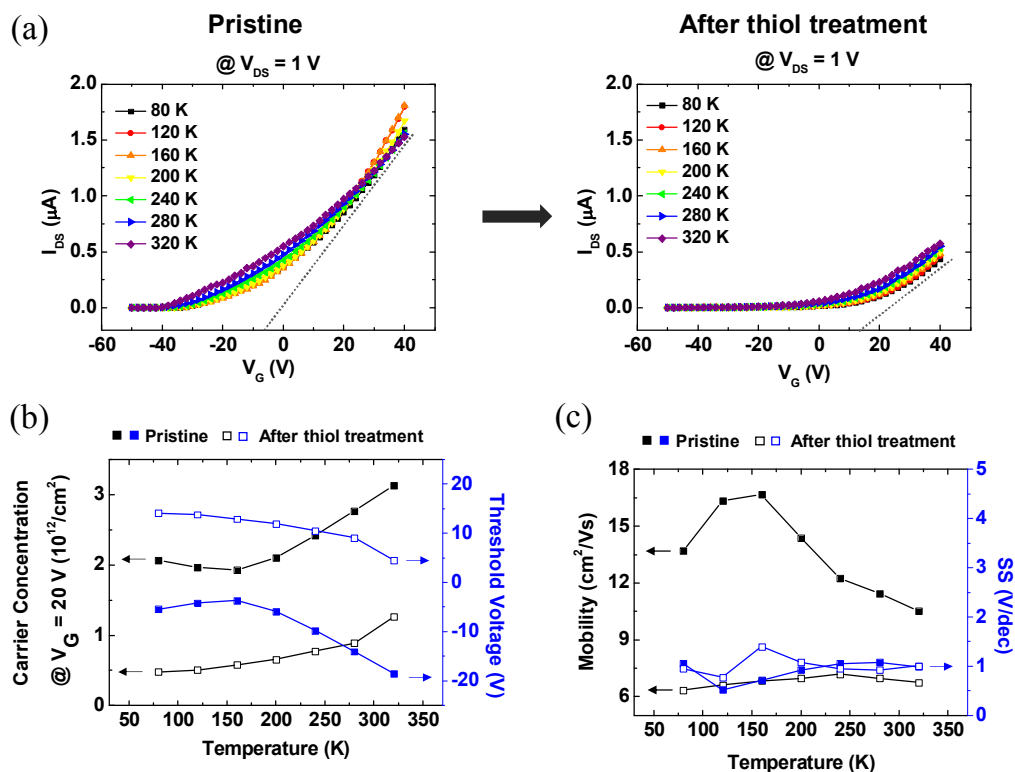


Figure 3.15 (a) I_{DS} - V_G curves measured before and after hexadecanethiol treatment with varying temperature from 80 to 320 K. (b) Carrier concentration and threshold voltage of a MoS₂ FET as a function of temperature acquired before and after the hexadecanethiol treatment. (c) Mobility and SS value of a MoS₂ FET as a function of temperature acquired before and after the hexadecanethiol treatment.

of 20 V. We can see that the carrier concentration dramatically decreased and the threshold voltage dramatically shifted to the positive gate voltage direction after the molecule treatment.

We also estimated the mobility and SS value of the device and the results are summarized in Figure 3.5(c). We observed that there was no significant difference in SS values before and after the molecule treatment. The SS value is related with the number

of trap sites. If the number of trap sites increases, the SS value would increase. However, the SS value did not change significantly after the molecule treatment, which means that the thiol molecules would not mainly act as trap sites, instead it is more likely that the molecules are passivating sulfur vacancies and decreasing the carrier concentration. In other words, although both the molecules acting as trap sites and the molecules passivating sulfur vacancies and decreasing the carrier concentration can be the reason of the source-drain current reduction, but the passivating effect from absorbed alkanethiol molecules seems to be a more dominant effect of the current reduction phenomenon. Furthermore, the SS value did not vary significantly as temperature was varied. This also supports our interpretation. Note that the mobility of the device decreased after the molecule treatment. This can be explained by a hopping transport model.[22] Electrons in the MoS₂ can transport through the sulfur vacancy sites by hopping. With this model, the average distance between the sulfur vacancy sites would increase after the molecule treatment by passivating sulfur vacancy sites of MoS₂. Therefore, it will make the hopping probability decrease and mobility decrease as well. Note that if the behavior of Ti-MoS₂ contact were changed after the molecule treatment, it would change the electrical properties of the devices. However, the contact effect cannot be the dominant reason for our observation. For example, we calculated the effective barrier height with the following formula for a 2D transport channel, $\ln\left(\frac{I_{DS}}{T^2}\right) = -\left(\frac{e}{k_B T}\right)\phi_B + const.$ ⁴² With this calculation, the effective barrier height was estimated to be changed by ~0.03 meV after the molecule treatment (at V_G = 40 V), which indicates that the contact effect would not be significant in our study. And, also note that the characteristics of contacts between MoS₂ and Ti electrode are not determined by just comparing Fermi levels of Ti and MoS₂. [41] The sulfur vacancy causes the E_F of MoS₂ to increase and this result leads to a

narrow Schottky barrier for the Ti/MoS₂ contact with sulfur vacancy.[41] In our case, we treated alkanethiol molecules after the device fabrication. Therefore, the Ti/MoS₂ contact region was already covered by Ti and the alkanethiol molecules were absorbed on the channel only, but not on the Ti/MoS₂ contact region. Besides, the alkanethiol molecules cannot form self-assembled monolayer on Ti surface, so molecule treatment makes no change in the electronic properties of Ti. Therefore, the contact behavior would not be changed before and after the molecule treatment.

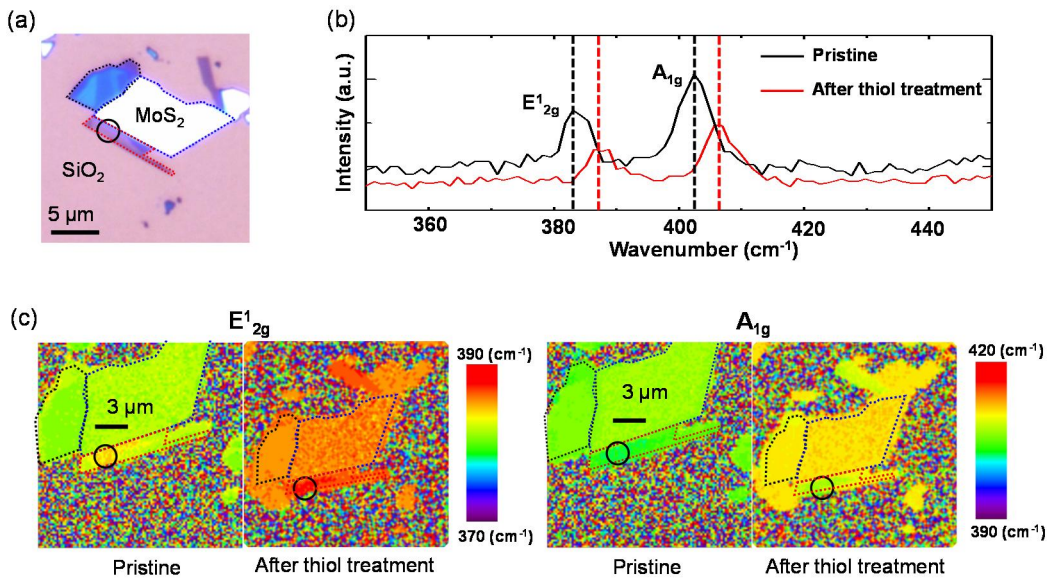


Figure 3.16 (a) The optical image of a MoS₂ flake that was used for Raman and PL studies. (b) The Raman spectra measured from a circled region marked in (a) before and after the hexadecanethiol treatment. (c) The Raman mapping image of E_{12g}¹ mode and A_{1g} mode before (left) and after (right) the hexadecanethiol treatment. We added dotted lines to indicate the MoS₂ flakes in this figure.

3.3.3. Optical properties of MoS₂ FETs with Thiol molecule treatment

If a MoS₂ surface is covered with molecules, then the vibration characteristics of a MoS₂ film will be altered. Because Raman spectroscopy has been used as a powerful tool in studying two-dimensional materials, we measured and compared the Raman spectrum of a MoS₂ flake prior to and after alkanethiol treatment under the same conditions. We used a Raman system with a ~1 mW, 532 nm wavelength laser. With the Raman spectroscopic study, one can find two characteristic normal modes of vibration in MoS₂, an E¹_{2g} mode and an A_{1g} mode. The E¹_{2g} peak in the Raman spectrum is the result of in-plane vibrations of Mo atoms and S atoms in opposite directions, and the A_{1g} mode is associated with the S atoms' out-of-plane vibration in the opposite direction. Figure 3.6(a) shows the optical image of a MoS₂ flake. We can approximately determine the thickness of the MoS₂ flake from the contrast of the optical image. The black circled region in Figure 3.6(a) is a single-layer MoS₂ flake piece. Figure 3.6(b) shows the Raman spectra of a single-layer MoS₂ flake before and after hexadecanethiol treatment. The black and red curves in Figure 3.6(b) were measured before and after the hexadecanethiol treatment, respectively. In the case of pristine MoS₂ flakes, *i.e.*, MoS₂ flakes prior to the hexadecanethiol treatment, E¹_{2g} and A_{1g} modes were observed at 383.0 cm⁻¹ and 402.3 cm⁻¹, respectively, which suggests that the circled region is indeed a single-layer MoS₂ flake (The difference of the E¹_{2g} and A_{1g} peak positions is 19.3 cm⁻¹).[36] An important finding is that both E¹_{2g} and A_{1g} modes shifted to a higher wavenumber (blue-shifted). The E¹_{2g} mode blue-shifted from 383.0 cm⁻¹ to 387.6 cm⁻¹ and the A_{1g} mode blue-shifted from 402.3 cm⁻¹ to 406.9 cm⁻¹. The blue-shift of the E¹_{2g} and A_{1g} modes can be explained by the molecule adsorption. The chemically adsorbed alkanethiol molecules on the MoS₂ surfaces slightly suppress atomic vibrations and lead to a higher force constant of vibration, causing the wavenumber blue-shift. Figure 3.6(c) displays the Raman spectra

mapping around the peak position of the E_{2g}^1 and A_{1g} modes. In this figure, we added dotted lines to indicate the MoS_2 flakes. After the alkanethiol treatment, the peak positions for both the E_{2g}^1 and A_{1g} modes in every part of the MoS_2 flakes shifted in the direction of higher wavenumbers. We also investigated the effect of another alkanethiol molecule, octanethiol ($\text{HS}(\text{CH}_2)_7\text{CH}_3$), on MoS_2 by comparing the Raman spectra mapping images of MoS_2 flakes before and after treatment with octanethiol. The results demonstrated that a blue-shift in the Raman data was consistently observed in this case as well, which suggests that the changed effect is due to the sulfur-containing thiol molecules. And, note that the Raman spectra of the MoS_2 flakes did not change noticeably when they were treated with only ethanol solution that did not contain alkanethiol molecules. Furthermore, when we continued to deposit alkanethiols on the

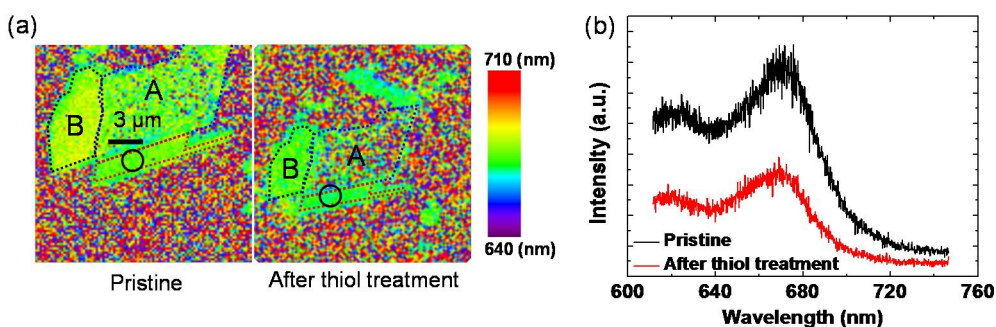


Figure 3.17 (a) PL peak position mapping image of the MoS_2 flake shown in Figure 4(a) before (left) and after (right) the hexadecanethiol treatment. (b) PL spectra measured from a circled region before and after the hexadecanethiol treatment. We added dotted lines to indicate the MoS_2 flakes in this figure.

MoS_2 flakes that had been treated with ethanol, we consistently observed the blue-shift phenomenon in Raman spectra. All these observations suggest that the alkanethiol molecules are the main reason for the blue-shift in the Raman data of the MoS_2 flakes and for the changes in the electrical parameters in the MoS_2 FETs.

In addition to Raman spectroscopy, we also measured the photoluminescence spectra of MoS₂ before and after the hexadecanethiol treatment. Notice that MoS₂ can be affected by the incident laser's polarization of PL, known as a valley polarization phenomenon in MoS₂,^[37] we did not use any polarization filter in order to prevent unwanted effect from the valley polarization. Figure 3.7(a) shows the PL mapping image of pristine MoS₂ flakes (left image) and hexadecanethiol-treated MoS₂ flakes (right image). Figure 3.7(b) displays the PL spectra that were acquired from the circled regions shown in Figure 3.7(a). Generally, two resonance peaks can be observed in the PL spectra of MoS₂ flakes at ~ 625 nm and ~ 670 nm, which are due to the spin-orbital splitting of the valence band and direct excitonic transitions in MoS₂, respectively.^[38] We observed that with the hexadecanethiol treatment, the PL peaks shifted slightly from 621 nm to 618 nm and from 673 nm to 668 nm and that the intensity of the PL peak decreased noticeably (Figure 3.7(b)). Moreover, the PL peak signals from the interband transition in the bulk MoS₂ flake region (marked with A) disappeared, and those in the multilayer MoS₂ flake region (marked with B) shifted from a yellow to a green color, *i.e.*, to the smaller wavelength direction (Figure 3.7(a)), which indicates that the PL peaks shifted in a high energy direction. This phenomenon can be explained as follows; generally the PL peak depends on the energy band structure of materials. In MoS₂, a sulfur vacancy provides an electron donor level within the band gap of MoS₂.^[22] Now, when we treat the MoS₂ with alkanethiol molecules, the number of donor levels in the band gap of MoS₂ decreases by passivating the sulfur vacancy sites of MoS₂ with the alkanethiol molecules. As a result, the intensity of the PL spectrum decreases and the peak position shifts slightly to the high

energy direction. And note that because the PL peak shift is slight, so that it can be considered that the band gap of MoS₂ was not changed noticeably by the alkanethiol molecule treatment. As a comparison experiment, we measured the PL spectra on MoS₂ flakes that were treated with ethanol solution without alkanethiol molecules. The result was that the PL spectra of the ethanol-treated MoS₂ flakes did not change noticeably. Additionally, to further verify chemisorption of alkanethiol molecules on the surface of MoS₂, we measured the binding energy of MoS₂ prior to and after the hexadecanethiol molecule treatment using an X-ray photoelectron spectroscopy (XPS) system. The result was that the XPS characteristic peaks' positions of the MoS₂ shifted after the alkanethiol molecule treatment, which indicates that the chemical environment of the MoS₂ was indeed changed.

3.3.4. Thickness and surface area dependence

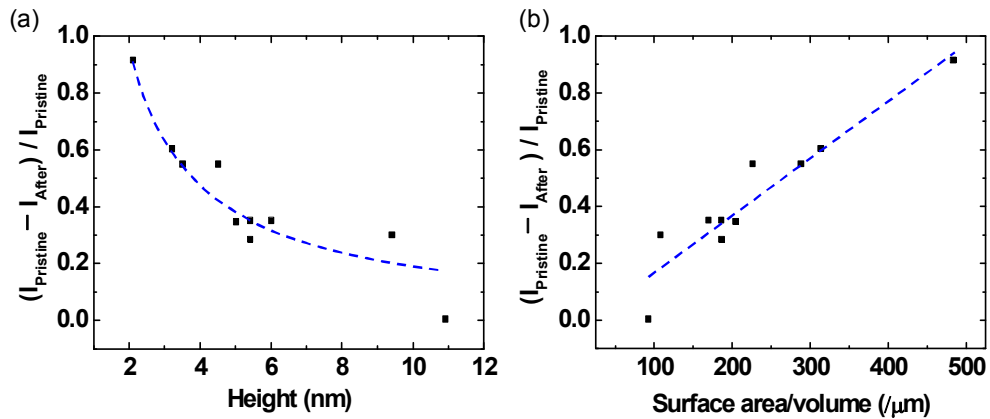


Figure 3.18 (a) Difference in channel currents measured before (I_{Pristine}) and after (I_{After}) the hexadecanethiol treatment for ten MoS₂ FET devices with different layer thicknesses (height) of the MoS₂ channel. (b) Difference channel currents before and after hexadecanethiol treatment as a function of the surface area to volume ratio of the MoS₂ channel film. The blue dashed lines were added to demonstrate the dependence of the channel current difference on the MoS₂ channel's height or surface area to volume ratio.

As we discussed above, alkanethiol molecules can be chemically absorbed at the sulfur vacancy sites on the surface of MoS₂, and this is the reason for the current decrease, the threshold voltage shift, the Raman peak shift, and the changes in PL spectra with the treatment by the thiol molecules. The number of sulfur vacancy sites depends on the surface area of the MoS₂ channel. Thus, the effect of alkanethiol molecules depends on the surface area of the MoS₂ channel. Additionally, this effect depends on the thickness of the MoS₂ flakes because MoS₂ is a two-dimensional layered material and the height is a major factor in determining the surface to volume ratio of the MoS₂ layer. Figure 3.8(a) displays the current difference *versus* height data plot. We measured the channel current for all the MoS₂ FET devices that we fabricated, and calculated the current difference as $(I_{\text{Pristine}} - I_{\text{After}})/I_{\text{Pristine}}$. Here, I_{Pristine} and I_{After} are the current levels of the devices that were measured at $V_G = 20$ V and $V_{\text{DS}} = 0.5$ V prior to and after the alkanethiol treatment. For this study, we fabricated a total of ten MoS₂ FET devices that were prepared from mechanically exfoliated MoS₂ flakes, of which the thickness varied from 2 to 11 nm. As can be observed in the plot of Figure 3.8(a), the current difference is proportional to the inverse of the thickness of the MoS₂ channel. The blue dashed curve in this plot was added to show this dependence. Figure 3.8(b) displays the plot of the current difference *versus* the surface area to volume ratio. We calculated the values of surface area to volume ratio as $(2hl + wl)/hwl$, where h is the thickness of the MoS₂ channel, w is the channel width and l is the channel length. As shown in Figure 3.8(b), the current difference of the MoS₂ FETs depended on the MoS₂ channel's surface to volume ratio. The results in Figure 3.7 show that the effect of the alkanethiol adsorption to the MoS₂ surface on the channel current of MoS₂ FETs decreases as the thickness of the MoS₂

channel increases (*i.e.*, the surface area to volume decreases). We also calculated the carrier concentration difference and mobility difference of the characterized MoS₂ FET devices.

3.3.5. Energy band schematic

We now explain the effect of alkanethiol molecule adsorption on the MoS₂ surface using the energy band diagrams as shown in Figure 3.9. Figure 3.9(a) and 3.9(b) show the energy band diagram before and after the alkanethiol absorption. The Ti metal as the source-drain electrode has a work function of ~ 4.3 eV, and MoS₂ has a work function in the range of 4.6 – 4.9 eV. However, although the work function of Ti is smaller than that of MoS₂, there is a Schottky barrier formed between the Ti and MoS₂. [39-41] Figure 3.9(b) shows energy band diagram after the alkanethiol molecule treatment. When the MoS₂ devices are treated with alkanethiol molecules, the alkanethiol molecules that are chemically adsorbed at the surface of MoS₂ can capture the electrons of unsaturated Mo in MoS₂ and deplete the MoS₂ channel. Thus, alkanethiol molecules

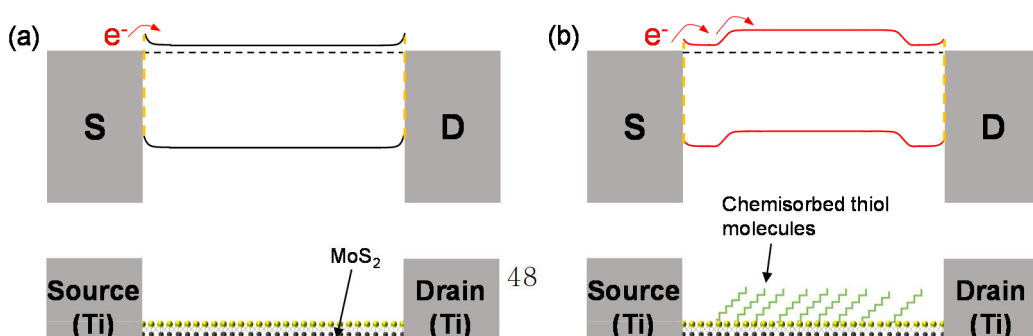


Figure 3.19 The schematics of the energy band diagram at $V_G = 0$ (a) before and (b) after the alkanethiol molecule treatment.

act as an energy barrier, resulting in the decrease of the channel current (Figure 3.4).

3.4. Conclusion

In summary, we fabricated MoS₂ FETs and measured their physical properties before and after alkanethiol molecule treatment to investigate the effect of passivating sulfur vacancy on the surface of MoS₂. After treatment with alkanethiol molecules, we observed that the source-drain current of the MoS₂ FETs decreased dramatically. In addition, the Raman spectrum peaks (E_{2g}^1 and A_{1g}) of MoS₂ flakes exhibited a blue-shift, and the PL peaks disappeared or slightly shifted after the alkanethiol treatment. From the temperature-variable electrical characterization, the changes in physical and electrical properties of MoS₂ flakes and MoS₂ FET devices are a result of the alkanethiol molecules capturing the electrons in MoS₂ by passivating sulfur vacancy sites (unsaturated Mo) on the MoS₂ surface. Our study may foster a way of tailoring the electrical and optical properties of MoS₂ by sulfur vacancy passivation using sulfur-containing molecules.

References

- [1] Novoselov, K.; Geim, A. K.; Morozov, S.; Jiang, D.; Zhang, Y.; Dubonos, S.; Grigorieva, I.; Firsov, A. *Science* **2004**, *306*, 666-669.
- [2] Novoselov, K. S.; Jiang, D.; Schedin, F.; Booth, T. J.; Khotkevich, V. V.; Morozov, S. V.; Geim, A. K. *P. Natl. Acad. Sci. U.S.A.* **2005**, *102*, 10451-10453.
- [3] Li, X.; Wang, X.; Zhang, L.; Lee, S.; Dai, H. *Science* **2008**, *319*, 1229-1232.
- [4] Allen, M. J.; Tung, V. C.; Kanar, R. B. *Chem. Rev.* **2010**, *110*, 132-145.
- [5] Xu, Y.; Bai, H.; Lu, G.; Li, C.; Shi, G. *J. Am. Chem. Soc.* **2008**, *130*, 5856-5857.
- [6] Radisavljevic, B.; Radenovic, A.; Brivio, J.; Giacometti, V.; Kis, A. *Nat. Nanotechnol.* **2011**, *6*, 147-150.
- [7] Fang, H.; Chuang, S.; Chang, T. C.; Takei, K.; Takahashi, T.; Javey, A. *Nano Lett.* **2012**, *12*, 3788-3792.
- [8] Kam, K.; Parkinson, B. *J. Phys. Chem.* **1982**, *86*, 463-467.
- [9] Mak, K. F.; Lee, C.; Hone, J.; Shan, J.; Heinz, T. F. *Phys. Rev. Lett.* **2010**, *105*, 136805.
- [10] Jariwala, D.; Sangwan, V. K.; Lauhon, L. J.; Marks, T. J.; Hersam, M. C. *ACS Nano* **2014**, *8*, 1102-1120.
- [11] Perkins, F. K.; Friedman, A. L.; Cobas, E.; Campbell, P. M.; Jernigan, G. G.; Jonker, B. T. *Nano Lett.* **2013**, *13*, 668-673.
- [12] Lee, H. S.; Min, S. W.; Park, M. K.; Lee, Y. T.; Jeon, P. J.; Kim, J. H.; Ryu, S.; Im, S. *Small* **2012**, *8*, 3111-3115.
- [13] Wang, H.; Yu, L.; Lee, Y. H.; Shi, Y.; Hsu, A.; Chin, M. L.; Li, L. J.; Dubey, M.; Kong, J.; Palacios, T. *Nano Lett.* **2012**, *12*, 4674-4680.
- [14] Yin, Z.; Zeng, Z.; Liu, J.; He, Q.; Chen, P.; Zhang, H. *Small* **2013**, *9*, 727-731.
- [15] Radisavljevic, B.; Whitwick, M. B.; Kis, A. *ACS Nano* **2011**, *5*, 9934-9938.
- [16] Choi, W.; Cho, M. Y.; Konar, A.; Lee, J. H.; Cha, G. B.; Hong, S. C.; Kim, S.; Kim, J.; Jena, D.; Joo, J. *et al. Adv. Mater.* **2012**, *24*, 5832-5836.
- [17] Li, H.; Yin, Z.; He, Q.; Li, H.; Huang, X.; Lu, G.; Fam, D. W. H.; Tok, A. I. Y.; Zhang, Q.; Zhang, H. *Small* **2012**, *8*, 63-67.
- [18] Kim, S.; Konar, A.; Hwang, W. S.; Lee, J. H.; Lee, J.; Yang, J.; Jung, C.; Kim, H.; Yoo, J. B.; Choi, J. Y. *et al. Nat. Commun.* **2012**, *3*, 1011.

- [19] Wu, S.; Huang, C.; Aivazian, G.; Ross, J. S.; Cobden, D. H.; Xu, X. *ACS Nano* **2013**, *7*, 2768-2772.
- [20] Eda, G.; Yamaguchi, H.; Voiry, D.; Fujita, T.; Chen, M.; Chhowalla, M. *Nano Lett.* **2011**, *11*, 5111-5116.
- [21] Lee, Y. H.; Zhang, X. Q.; Zhang, W.; Chang, M. T.; Lin, C. T.; Chang, K. D.; Yu, Y. C.; Wang, J. T. W.; Chang, C. S.; Li, L. J. et al. *Small* **2012**, *24*, 2320-2325.
- [22] Qiu, H.; Xu, T.; Wang, Z.; Ren, W.; Nan, H.; Ni, Z.; Chen, Q.; Yuan, S.; Miao, F.; Song, F.; Long, G.; Shi, Y.; Sun, L.; Wang, J.; Wang, X. *Nat. Commun.* **2013**, *4*, 2642.
- [23] Noh, J-Y.; Kim, H.; Kim, Y-S. *Phys. Rev. B* **2014**, *89*, 205417.
- [24] Makarova, M.; Okawa, Y.; Aono, M. *J. Phys. Chem. C* **2012**, *116*, 22411-22416.
- [25] Wiegenstein, C. G.; Schulz, K. H. *J. Phys. Chem. B* **1999**, *103*, 6913-6918.
- [26] Peterson, S. L.; Schulz, K. H. *Langmuir* **1996**, *12*, 941-945.
- [27] Cygan, M. T.; Dunbar, T. D.; Arnold, J. J.; Bumm, L. A.; Shedlock, N. F.; Burgin, T. P.; Jones II, L.; Allara, D. L.; Tour, J. M.; Weiss, P. S. *J. Am. Chem. Soc.* **1998**, *120*, 2721-2732.
- [28] Park, S.; Wang, G.; Cho, B.; Kim, Y.; Song, S.; Ji, Y.; Yoon, M. H.; Lee, T. *Nat. Nanotechnol.* **2012**, *7*, 438-442.
- [29] Kumar, A.; Whitesides, G. M. *Appl. Phys. Lett.* **1993**, *63*, 110628.
- [30] Poirier, G. E.; Tarlov, M. J. *Langmuir*, **1994**, *10*, 2853-2856.
- [31] Reed, M. A.; Zhou, C.; Muller, C. J.; Burgin, T. P.; Tour, J. M. *Science*, **1997**, *278*, 252-254.
- [32] Najmaei, S.; Zou, X.; Er, D.; Li, J.; Jin, Z.; Gao, W.; Zhang, Q.; Park, S.; Ge, L.; Lei, S.; Kono, J.; Shenoy, V. B.; Yakobson, B. I.; George, A.; Ajayan, P. M.; Lou, J. *Nano Lett.* **2014**, *14*, 1354-1361.
- [33] Cho, K.; Park, W.; Park, J.; Jeong, H.; Jang, J.; Kim, T. Y.; Hong, W. K.; Hong, S.; Lee, T. *ACS Nano*, **2013**, *7*, 7751-7758.
- [34] Park, W.; Park, J.; Jang, J.; Lee, H.; Jeong, H.; Cho, K.; Hong, S.; Lee, T. *Nanotechnology*, **2013**, *24*, 095202.
- [35] Das, H.; Chen, H-Y.; Penumatcha, A. V. Appenzeller, J. *Nano Lett.* **2013**, *13*, 100-105.
- [36] Li, H.; Zhang, Q.; Yap, C. C. R.; Tay, B. K.; Olivier, T. H. T. E. A.; Baillargeat, D. *Adv. Funct. Mater.* **2012**, *22*, 1385-1390.

- [37] Zeng, H.; Dai, J.; Yao, W.; Xiao, D.; Cui, X. *Nat. Nanotechnol.* **2012**, *7*, 490-493.
- [38] Splendiani, A.; Sun, L.; Zhang, Y.; Li, T.; Kim, J.; Chim, C. Y.; Galli, G.; Wang, F. *Nano Lett.* **2010**, *10*, 1271-1275.
- [39] Feng, L. P.; Su, J.; Liu, Z. T. *J. Alloy. Compd.* **2014**, *613*, 122-127.
- [40] Kang, J.; Lue, W.; Banerjee, K. *Appl. Phys. Lett.* **2014**, *104*, 233502.
- [41] Feng, L. P.; Su, K.; Li, D. P.; Liu, Z. T. *Phys. Chem. Chem. Phys.* **2015**, *17*, 6700.
- [42] Wang, W.; Liu, Y.; Tang, L.; Jin, Y.; Zhao, T.; Xiu, F. *Sci. Rep.* **2014**, *4*, 6928
Reed, M. A.; Zhou, C.; Muller, C. J.; Burgin, T. P.; Tour, J. M. *Science* **1997**, *278*, 252-254.

Chapter 4. Electrical Properties of MoS₂ FETs with Contact Treatment by Thiol Molecules

In this chapter, we introduce a new approach for obtaining modified contact properties by inserting thiol molecules between metal electrode and MoS₂ channel. Although two-dimensional (2D) molybdenum disulfide (MoS₂) has gained much attention due to its unique electrical and optical properties, the limited electrical contact to 2D semiconductors still impedes to realize high-performance 2D MoS₂-based devices. In this regard, many studies have been conducted to improve the carrier injection properties by inserting functional paths, such as graphene or hexagonal boron nitride, between electrodes and 2D semiconductors. The reported strategies, however, require relatively time-consuming and low-yield transfer processes on sub- μm MoS₂ flakes. Here, we suggest a simple contact-engineering method, introducing chemically adsorbed thiol-molecules as thin tunneling barriers between the metal electrodes and MoS₂ channels. The selectively deposited thiol-molecules via the vapor-deposition process provide additional tunneling paths at the contact regions, improving the carrier injection properties with lower activation energies in MoS₂ field-effect transistors. Additionally, by inserting thiol-molecules at the only one contact region, asymmetric carrier-injection was feasible depending on the temperature and gate bias.

4.1. Introduction

Molybdenum disulfide (MoS₂), widely studied as a two-dimensional (2D) semiconducting material in the transition dichalcogenides (TMDs) family, has unique properties including good flexibility, transparency, a tunable bandgap energy controlled by the number of layers, and spin-valley physics from the strong internal magnetic field.[1-9] Due to its fascinating characteristics, MoS₂ has received much attention for the

realization of promising nanoelectronics and optoelectronics. However, delivering good contact properties between 2D semiconductors and metal electrodes is still challenging, and this is essential to achieve excellent electrical and optical performances especially in the low-operation voltage regimes. Theoretically, it is predicted that a much lower contact resistance (three orders of magnitude) in MoS₂ devices might be achieved compared to the previously reported experimental values.[10] Therefore, many research groups have proposed emerging methods to improve contact properties, for example, inserting functional layers between 2D semiconductors and electrodes,[11,12] thermal annealing at contact regions,[13] phase engineering with high-energy beam irradiation,[14] and employing graphene electrodes[15,16] low-work function metals,[17,18] or a direct CVD-growth method of 2D heterostructures in lateral.[19,20] However, thermal annealing and high-energy beam irradiation may damage 2D materials, and direct CVD-growth method of lateral 2D heterostructures is difficult to define accurate junction areas between 2D materials. Therefore, more facile approach to improve the contact properties between metal electrodes and 2D semiconductors is desired for the typical 2D field-effect transistor structure.

Among these methods, introducing a thin tunneling barrier between the MoS₂ channel and electrodes is an efficient approach to improve contact properties by reducing the activation energy.[12,21,22] For example, graphene or hexagonal boron nitride (h-BN) have been vertically employed between metal contacts and 2D semiconductors as a thin tunneling barrier for the lower contact resistance.[21,22] Moreover, the use of cobalt electrodes facilitated Ohmic contact even in the extremely low temperature regime.[12] However, relatively complex, high-cost, and low-yield transfer processes were required to make vertically stacked 2D heterostructures.[11,12] Additionally, it is difficult to

introduce atomically thin tunneling barriers using conventional transfer methods to the exact contact location on flake-type MoS₂ with dimensions of sub- μm size. Here, we demonstrate a simple strategy for inserting a thin tunneling barrier by depositing thiol-molecules between MoS₂ semiconductors and conventional metal electrodes. Vaporized thiol-molecules are chemically adsorbed on MoS₂ with covalent bonding. The inserted thiol-molecules at the contact region create additional tunneling paths, resulting in a drastically reduced activation energy; therefore, the primary injection mechanism of the contact-engineered MoS₂ field-effect transistors (FETs) changes from thermionic emission to field emission, allowing better contact properties without a temperature dependency. In addition, by defining contact regions on MoS₂ using conventional lithography, where injection engineering is desirable, a selective introduction of thiol-molecules is feasible with $\sim 100\%$ yield that could support asymmetric carrier injection in FET device applications.

4.2. Experiments

4.2.1. Device fabrication process with inserted thiol molecules

Figure 4.1(a) shows the schematic images of the fabrication process of MoS₂ FETs with adsorbed thiol-molecules at the contact regions. MoS₂ flakes were transferred

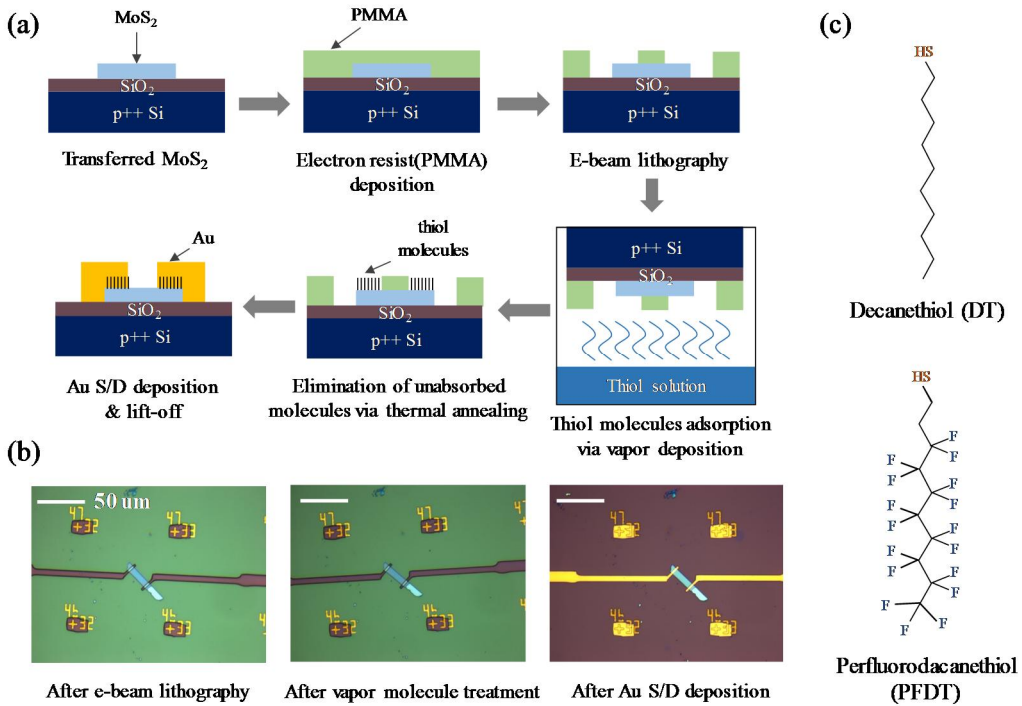


Figure 4.1. (a) Schematic images of the device fabrication process. (b) Optical images of the MoS₂ FETs during the fabrication process. (c) Schematics of the decanethiol (DT) and perfluorodecanethiol (PFDT) molecule.

on a cleaned *p*-type heavily doped Si substrate (resistivity $\sim 5 \times 10^{-3} \Omega \text{ cm}$) with 270 nm-thick SiO₂ with a mechanical exfoliation method. After the polymethyl methacrylate (PMMA, molecular weight of 4950 k/mol, 11% dissolved in anisole) electron resist polymer was spin-coated on the MoS₂ channel layer, the source/drain (S/D) patterns were defined using an electron beam lithography system (JSM-6510, JEOL). In addition, we deposited thiol-molecules (decanethiol or perfluorodecanethiol) via a vapor deposition method on the exposed contact region of the MoS₂ flake.

Thiol-molecules are chemically adsorbed at the sulfur vacancies of MoS₂ by generating a covalent bond with Mo.[23-28] In general, functional molecules have been deposited by dipping MoS₂ samples into thiol-based solution. However, this approach requires a long duration, and the PMMA barrier patterns used to define the S/D electrodes are easily damaged by the thiol solution. Therefore, we employed a vapor deposition method that did not destroy the PMMA patterns and allowed a selective deposition of the thiol-molecules on the specific MoS₂ contact regions (Figure 4.1(b)). The MoS₂ sample attached at the lid of a vial was exposed to vaporized thiol-molecules in the vial containing thiol solution. Note that the solution was heated up to 70 °C and the processes were performed in a N₂ glove box for 3 hours. Then, the thiol-deposited MoS₂ sample was annealed on a 70 °C hot plate for 1 hour to remove residual solvent. After the annealing process, 30 nm-thick Au was deposited as S/D electrodes using an electron beam evaporating system (KVE-2004L, Korea Vacuum Tech.). The stability of deposited thiol-molecules is discussed in the Supporting Information. Figure 4.1(b) shows the optical images of the MoS₂ FETs with the aforementioned procedure. The left image of Figure 4.1(b) shows that only the contact regions of MoS₂ were exposed for the thiol-molecule deposition with the development process, and the MoS₂ channel region was protected by the PMMA layer. After the thiol-molecule vapor deposition process, the PMMA patterns were not destroyed by the thiol-molecule vapor (see the middle image of Figure 4.1(b)). After the Au deposition, the chemically adsorbed thiol-molecules were located between the Au S/D electrodes and the MoS₂ surface. The detailed fabrication process is explained in the Experimental section. Figure 4.1(c) shows two types of thiol-molecules that are used in this study; one was decanethiol (DT) and the other was perfluorodecanethiol (PFDT). Both the DT and PFDT molecules have a similar molecular

length, with 10 carbon chains that introduce similar tunneling path length for carriers; however, these molecules have an opposing electric dipole moments due to fluorides in PFDT, which may affect the Schottky barrier height. We will discuss this in detail later.

4.2.2. Characterization of deposited thiol-molecules

Electron energy loss spectroscopy (EELS) data and energy-filtered TEM (EFTEM) images were taken by using a high-resolution transmission electron microscope (HRTEM) system (JEM-2100F, JEOL). For the preparation of the MoS₂ samples, we used a platinum layer as a protective layer for the focused ion beam (FIB) (Quanta 3D FEG, FEI) to prevent carbon contamination. In addition, an XPS (AXIS-SUPRA, KRATOS) mapping image (100 μm × 100 μm) and XPS spectra were obtained to investigate the deposited thiol-molecules. Raman mapping was measured using an XperRam 200 (Nanobase, Inc.) system equipped with a 532-nm laser and a power of 100 μW.

4.2.3. Activation energy extraction

The activation energy of the devices can be extracted from output curves measured under various temperature. We extracted the activation energies of the untreated and thiol-treated MoS₂ FETs from the output curves using the following equation for thermionic emission in 2D semiconducting system, $I_{DS} = A^*T^{\frac{3}{2}}\exp[(-q/k_B T)(E_A - V_{DS}/\eta)]$, where A^* , E_A , and η denote the Richardson coefficient, the effective activation energy, and ideality factor, respectively. First, we measured output characteristics of MoS₂ FETs under various temperature. Then, we plotted $\ln(I_{DS}/T^{\frac{3}{2}})$ vs $\frac{1}{T}$ curves varying V_{DS} . Then, the slope was extracted and plotted as

a function of V_{DS} . The y-intercept value indicates the effective activation energy.

4.2.4. Contact resistance extraction by using Y-function method

The Y-function method has been generally used to evaluate the contact resistance in low V_{DS} linear regime ($V_{GS} - V_{th} \gg V_{DS}$) for various materials such as carbon nanotube (CNT), organic materials and MoS₂ FETs.

If the additional voltage drop due to contact resistance is considered, I_{DS} in a linear regime can be expressed as

$$I_{DS} = \frac{\mu_0}{1+\theta_{ch}(V_{GS}-V_{th})} C_i \frac{W}{L} (V_{GS} - V_{th})(V_{DS} - I_{DS}R_C)$$

$$\Rightarrow I_{DS} = \frac{\mu_0}{1+\theta(V_{GS}-V_{th})} C_i \frac{W}{L} (V_{GS} - V_{th})V_{DS} ,$$

where μ_0 , θ_{ch} , C_i , W , L , R_C , V_{th} , θ , and denote the intrinsic mobility in linear regime, the mobility attenuation factor from channel, capacitance between the channel and the gate per unit area, the channel width, the channel length, the contact resistance, the threshold voltage and the mobility attenuation factor from both of channel and contact, respectively.

From the definition of transconductance ($g_m = \partial I_{DS}/\partial V_{GS}$), the Y-function is given by

$$Y = \frac{I_{DS}}{\sqrt{g_m}} = \frac{I_{DS}}{\sqrt{I_{DS}/(1+\theta(V_{GS}-V_{th}))}(V_{GS}-V_{th})}} = \sqrt{\mu_0 C_i V_{DS} \frac{W}{L}} (V_{GS} - V_{th}) .$$

From the slope of the Y-function versus V_{GS} , the value of $\sqrt{\mu_0 C_i V_{DS} W/L}$ can be extracted. The attenuation factor θ can be described as following equation.

$$\theta = \theta_{ch} + \theta_c = \theta_{ch} + \mu_0 C_i R_C \frac{W}{L} ,$$

where θ_c is the mobility attenuation factor from the contact.

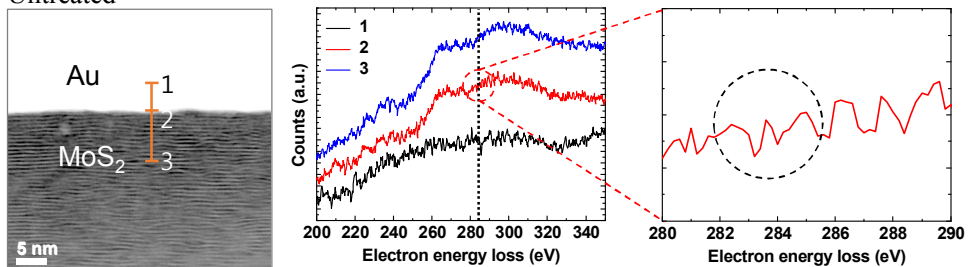
4.3. Results & Discussions

4.3.1. HRTEM and EELS analysis

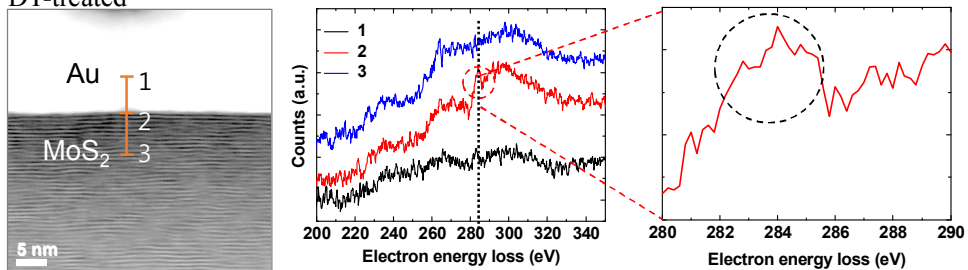
To verify that the thiol-molecules can be well adsorbed on the MoS₂ surface via the vapor deposition method, electron energy loss spectroscopy (EELS) with a high-resolution transmission electron microscope (HRTEM) (JEM-2100F, JEOL) was conducted for MoS₂ flakes without the thiol treatment (“untreated”), with DT treatment, and with PFDT treatment. Figure 4.2(a) shows the HRTEM cross-section image (left

panel) of the contact region and the EELS results (middle panel) measured at the Au electrode (position 1), the interface between the Au electrode and the MoS₂ (position 2), and the MoS₂ layer (position 3).

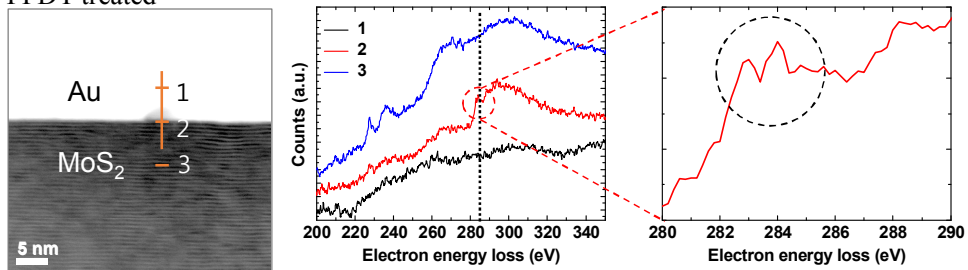
(a) Untreated



(b) DT-treated



(c) PFDT-treated



The magnified EELS profiles for position 2 are shown in the right panel of Figure 4.2(a). Figures 4.2(b) and 4.2(c) show the results of HRTEM cross-section images and EELS results for DT-treated MoS₂ and PFDT-treated MoS₂, respectively. From the magnified EELS profiles, the carbon peaks were clearly observed at the interface of DT and PFDT-treated MoS₂ at an electron energy of 284 eV, whereas they were not detected at the other positions and the interface of untreated MoS₂. Because the carbon peaks originated from the thiol-molecules adsorbed at the MoS₂ surface, these results support that thiol-molecules were inserted directly via the vapor treatment with the DT and PFDT solution between the MoS₂ layer and electrodes.

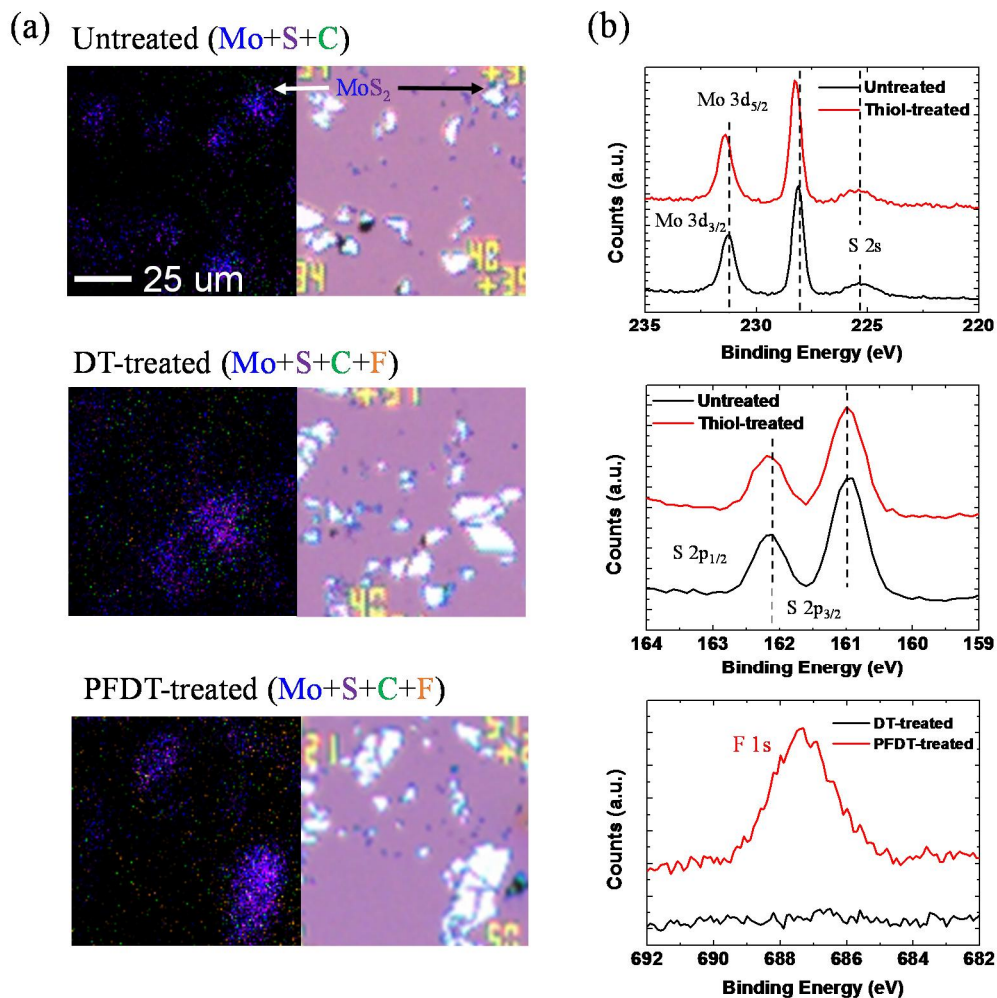
4.3.2. XPS analysis

Figure 20 (a) (left) HRTEM image of untreated MoS₂ sample, (middle) EELS data along the orange line in the HRTEM image at position 1, 2, and 3 and (right) magnified EELS data at position 2. b) (left) HRTEM image of DT-treated MoS₂ sample, (middle) EELS data along the orange line in the HRTEM image at position 1, 2, and 3 and (right) magnified EELS data at position 2. c) (left) HRTEM image of PFDT-treated MoS₂ sample, (middle) EELS data along the orange line in the HRTEM image at position 1, 2, and 3 and (right) magnified EELS data at position 2.

For the further investigation of the adsorbed thiol-molecules on MoS₂, X-ray photoelectron spectroscopy (XPS) (AXIS-SUPRA, KRATOS) was conducted on the prepared MoS₂ flakes. Figure 4.3(a) shows the optical and corresponding XPS mapping images of untreated, DT-treated, and PFDT-treated MoS₂ flakes. The positions where Mo, S, carbon (C), and fluorine (F) elements were adsorbed are indicated in blue, violet, green,

and orange, respectively. As expected, in the DT- or PFDT-treated MoS₂ flakes, the C peaks were more dominantly detected compared to the untreated MoS₂ flakes.

In addition, the intensity of the F peaks significantly increased on the PFDT-



treated MoS₂, which is consistent with the XPS results at the binding energy of 687 eV (bottom panel Figure 4.3(b)). In Figure 4.3(b), the characteristic peaks of Mo and S in DT-treated MoS₂ slightly shifted to the low-energy direction whereas those of PFDT-treated MoS₂ shifted to the opposite direction toward the high-energy direction, which is due to the opposite dipole moment directional configuration between the DT and PFDT thiol-molecules.

Figure 4.3 (a) XPS mapping image and optical image of (top) untreated, (middle) PFDT-treated, and (bottom) DT-treated MoS₂. Blue dots are the position where the Mo peak was observed in XPS, purple dots represents S, green dots represents C, and orange dots represents F. b) XPS data of untreated and thiol-treated MoS₂.

Therefore, the peak shift of XPS would be attributed to surface dipole from the chemisorbed thiol molecules rather than the change in core level of MoS₂.^[26] The energy-filtered TEM images at the MoS₂ surface and Raman mapping images also indicate that the thiol-molecules were well adsorbed selectively on the surface of MoS₂ via the vapor-deposition method.

4.3.3. The effect of the thiol-molecule inserted at the contact region

To investigate the effect of the thiol-molecules inserted at the contact regions on the electrical characteristics of MoS₂ FETs, especially on the carrier injection properties, we measured the output curves (source-drain current versus source-drain voltage; $I_{DS}-V_{DS}$) at a fixed gate voltage (V_{GS}) of 40 V for untreated, DT-treated, and PFDT-treated MoS₂ FETs under various temperatures ranging from 80 K to 300 K (Figure 4.4(a)). Note that all the measurements were executed in vacuum ($\sim 10^{-3}$ Torr) to avoid unwanted effects caused by oxygen and water molecules. For the untreated MoS₂ FETs, I_{DS} increased as temperature increased, whereas that of the thiol-treated MoS₂ FETs was maintained or slightly decreased as temperature increased, as shown in Figure 4.4(a). Moreover, the output curves of untreated MoS₂ FETs exhibited an obvious *S*-shaped curve at the low V_{DS} regime, which is typically observed if the Schottky contact is formed between a metal electrode and a semiconducting layer.

However, the thiol-treated FETs exhibited linear-shaped curves corresponding to the Ohmic contact behaviors even at a low temperature of 80 K. The change in the carrier injection behaviors can be explained by the effect of the inserted thiol-molecules. The carrier injection properties of the untreated MoS₂ FETs were determined by the Schottky

barrier as well as a tunneling barrier due to the van der Waals (vdW) gap that is naturally formed between the MoS₂ channel and Au electrode (left panel, Figure 4b).[29,30]

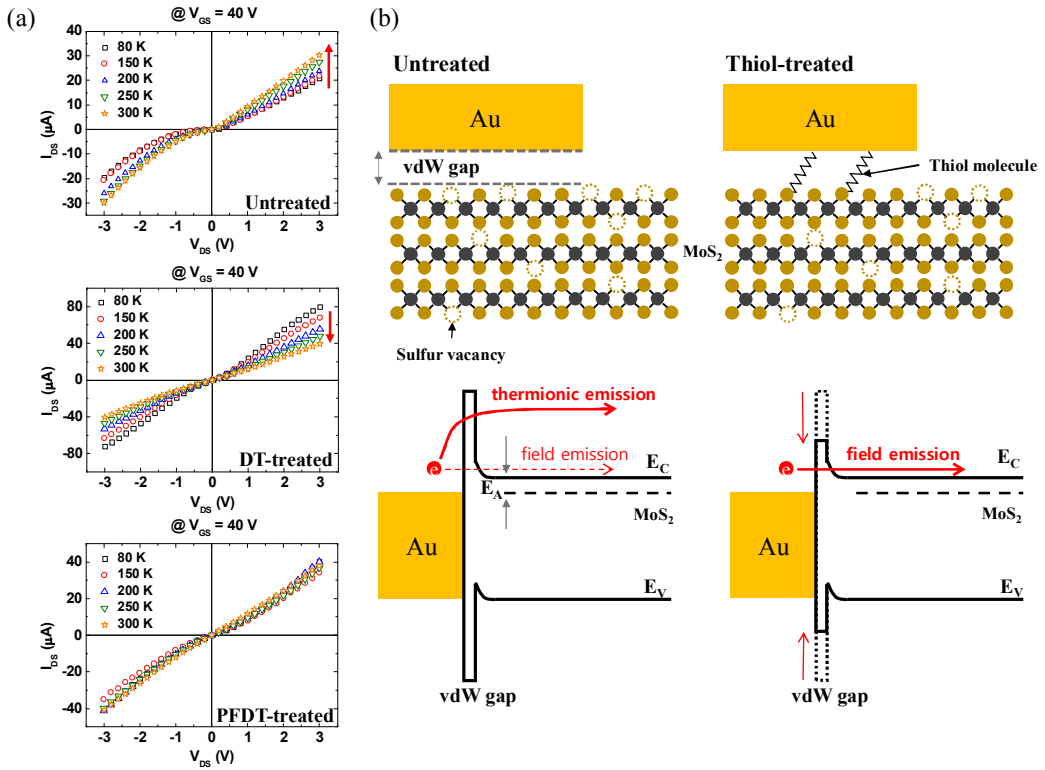


Figure 4.4 (a) Output curves with varying temperature from 80 K to 300 K of (top) untreated, (middle) DT-treated, and (bottom) PFDT-treated MoS₂ FETs at fixed gate bias. (b) (top) Contact and (bottom) energy band schematic for (left) untreated and (right) thiol-treated MoS₂.

Because of the Schottky barrier and tunneling barrier, the carriers must have enough activation energy to overcome those barriers to be injected from the metal electrodes to the MoS₂. Consequently, the primary carrier injection mechanism of untreated MoS₂ FETs was thermionic emission resulting in the temperature-dependent I_{DS} and carrier injection behaviors (top panel, Figure 4.4(a)). Farmanbar et al. reported that the inserted 2D buffer monolayer layer could interact with the transition metal reducing its work function. Additionally, it can impede the metal-TMD interaction to remove the interface states (such as sulfur vacancies) which cause the Fermi level pinning, rather than

preventing damage from metal evaporation or oxidation due to relatively low coverage of treated thiol molecules.[21,22] Similarly, for the thiol-treated MoS₂ FETs, the adsorbed thiol-molecules could remove the interface states that pinned the Fermi level in the MoS₂ band gap and create tunneling paths with an effectively lowered barrier at the interface and increased tunneling current through the junction. Therefore, the carriers can be injected more easily from the Au electrode to MoS₂ by field emission (tunneling) with much lower activation energy (bottom panels, Figure 4.4(b)). Note that although a slightly decreased I_{DS} was observed due to phonon scattering as the temperature increased, the carrier injection behaviors were insensitive to the temperature. The consistent temperature-dependent behaviors from the V_{DS} - I_{DS} curves were observed in both of the DT-treated MoS₂ FETs without and with the rinsing process. These results support that the primary carrier-injection mechanism changed from “Schottky-like contact” to “Ohmic-like contact” by inserting thiol-molecules with reduced effective activation energy. In addition, the contact resistance of our devices were evaluated. From the analysis using the Y-function method, the extracted value of contact resistances were found to be ~35.1 k Ω , 6.31 k Ω , and 22.6 k Ω for the untreated device, DT-treated device, and PFDT-treated device, respectively (the detailed explanation is provided in the Supporting Information). The normalized contact resistances considering different device geometry were estimated to be ~175.5 k $\Omega \cdot \mu\text{m}$, 25.2 k $\Omega \cdot \mu\text{m}$, and 67.7 k $\Omega \cdot \mu\text{m}$ for the untreated device, DT-treated device, and PFDT-treated device, respectively. The contact resistance values of the thiol-treated devices are smaller than those of the untreated devices. By the way, the contact resistance of our untreated device is in agreement with the reported values ($10^4 - 10^5 \Omega \cdot \mu\text{m}$).[30]

Note that sulfur vacancies of MoS₂ can be regarded as a critical factor to

determine electrical properties of MoS₂ FETs.[9,31-33] It was reported that pristine MoS₂ has ~3 % of sulfur vacancies.[34] These sulfur vacancies could be donor sites that can increase carrier concentration, resulting in increasing the channel conductance in MoS₂ FET systems.[9,31-33] On the other hand, sulfur vacancies located at contact regions introduce defects levels in the gap, leading to Fermi level pinning.[21,22] In this regards, only multilayer MoS₂ flakes (>20 nm thick) were used as a channel layer to prevent unwanted electrical degradation in this study.[33] And, we introduced thiol-molecules on the sulfur vacancies only at the contact regions, which could eliminate the interfacial states by passivating the sulfur vacancies and create additional tunneling paths through the chemisorbed thiol molecules.

4.3.4. Electrical characterization of MoS₂ FETs with asymmetric contact



Figure 4.5 (a) Optical images of asymmetric MoS₂ FETs during the fabrication process.

(b) Output curves at different gate bias conditions at fixed temperature. The drain electrode is DT treated and the source electrode is untreated. (c) Output curves at different temperature conditions at a fixed gate bias. The drain electrode is DT treated and the source electrode is untreated. (d) Output curves at different temperature conditions at a fixed gate bias. The source electrode is DT treated and the drain electrode is untreated. (e) Extracted activation energies of untreated, DT-treated, PFDT-treated, and HDT-treated MoS₂ FETs at different gate bias conditions. Red region represents “thermionic emission dominant” and blue region represents “field emission dominant”. (f,g) Rectification ratio at V_{DS} of -3 V and 3 V in (f) different gate bias conditions at a fixed temperature and at (g) different temperature conditions at a fixed gate bias.

This carrier-injection engineering method enables asymmetric MoS₂ FETs with untreated and DT-treated contact regions by inserting thiol-molecules selectively via the vapor deposition. Figure 4.5(a) shows the optical images of the MoS₂ devices during the fabrication process to demonstrate asymmetric MoS₂ FETs. First, we fabricated the DT-treated MoS₂ FETs (left panel, Figure 4.5(a)). After defining the contact regions using electron-beam lithography, Au S/D electrodes were deposited on the MoS₂ region that was not treated with thiol-molecules (middle panel, Figure 4.5(a)). Then, the electrical properties of asymmetric MoS₂ FETs (right panel, Figure 4.5(a)) were characterized by measuring the channel current between the untreated and DT-treated contacts in vacuum under various temperatures ranging from 80 K to 300 K. Figure 4.5(b) shows the output curves of the asymmetric MoS₂ FETs with the DT-treated drain and untreated source electrodes measured at $V_{GS} = 40$ V (black empty symbols) and -20 V (blue filled symbols) at 300 K. At $V_{GS} = 40$ V, symmetric I_{DS} behaviors were exhibited in both the positive and negative V_{DS} regimes (Figure 4.5(b)). However, at a negative V_{GS} of -20 V, asymmetric I_{DS} behaviors were shown (Figure 4.5(b)), which can be explained by the activation energy difference between the untreated and DT-treated contacts. We extracted the activation energy of the untreated and thiol-treated MoS₂ FETs from the output curves using the following equation for thermionic emission in 2D semiconducting system, $I_{DS} = A^*T^2 \exp[(-q/k_B T)(E_A - V_{DS}/\eta)]$, where A^* , E_A , and η denote the Richardson coefficient, the effective activation energy, and ideality factor, respectively. From the extracted results, the effective activation energies of thiol-treated MoS₂ FETs were found to be much lower than those of untreated MoS₂ FETs due to the inserted thiol-molecules

(Figure 4.5e). Although DT and PFDT have opposing electric dipole moments, which could affect the work function and Schottky barrier height at the interface between the MoS₂ channel and contacts, both thiol-molecules delivered lowered activation energies regardless of the direction of the electric dipole moments. This result indicates that the thiol-molecules reduced the tunneling barrier with the creation of additional tunneling paths at the contact region, which is more dominant than the effect of their electric dipole moments. A previously reported result by Cheng et al. also supports that both DT and PFDT treatments could improve both the hole and electron injection properties of organic transistors by introducing tunneling paths between the metal electrodes and organic semiconducting layers even though the DT and PFDT have the opposite direction of electric dipole moments.[35] In addition, we applied hexadecanethiol (HDT) molecules, which have 16 carbon chains, on MoS₂ to investigate the effect of the carbon chain length. For the HDT-treated MoS₂ FETs, a much lower activation energy than that of the untreated MoS₂ FETs was also extracted, but it was slightly higher than those of DT or PFDT-treated MoS₂ FETs because of its longer carbon chain length. It is expected that a similar trend of tunneling behaviors will be observed if shorter molecules than DT are inserted.

For the MoS₂ FETs with the thiol treatment on one contact region, as the gate voltage decreased, the difference of the extracted activation energy increased such that the asymmetric current ratio at -3 V and 3 V also increased by ~20 times (Figure 4.5(e) and 4.5(f)). Moreover, while the carrier injection by thermionic emission through the untreated contact was affected by the temperature condition, the carrier injection through the DT-treated contact was insensitive to the temperature (see Figure 4.5(c) and 4.5(d)). Therefore, the symmetry in the MoS₂ FETs with the selectively thiol-treated contact

region was dependent on the temperature showing an increased asymmetric current ratio as the temperature decreased (Figure 4.5(g)). These results were enabled by carrier injection engineering from the thermionic emission to field emission

4.2.4. Energy band schematics of asymmetric devices

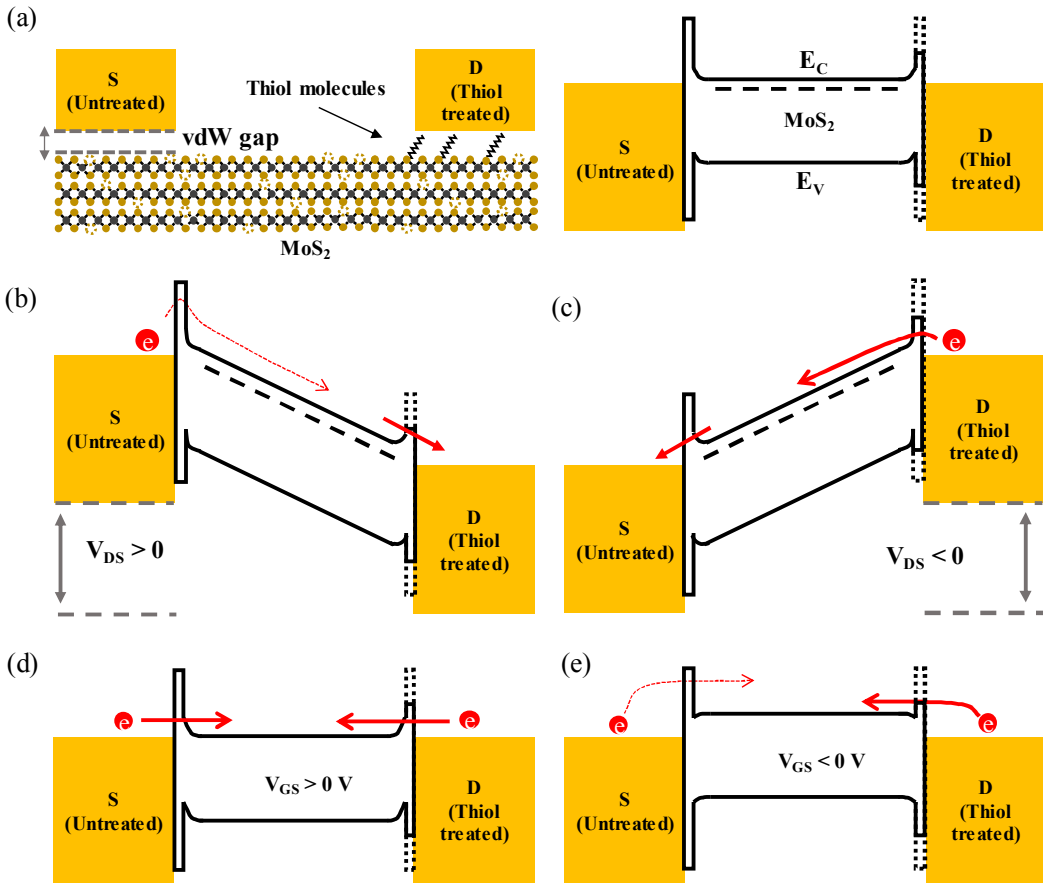


Figure 4.6 (a) Schematics of (left) device structures and (right) energy band diagram for asymmetric MoS₂ FETs. (b,c) Energy band diagram for (b) positively and (c) negatively biased source-drain condition. (d,e) Energy band diagram for (d) positively and (e) negatively biased gate condition.

Figure 4.6(a) shows the schematics of structures and energy band diagrams for asymmetric MoS₂ FETs. As mentioned earlier, the untreated Au source contact region has a van der Waals gap with the MoS₂ channel while selectively inserted DT molecules are placed between the MoS₂ channel and the Au drain electrode. Therefore, there are different tunneling barrier heights for the untreated and treated contact regions (right panel of Figure 4.6(a)). Because the carriers must be injected through the untreated barrier from the source electrode by thermionic emissions when $V_{DS} > 0$ V, the I_{DS} was affected by the temperature, as shown in Figure 4.6(b). However, at a negative V_{DS} , the carriers can transport through the extremely lowered barrier (the extracted activation energy was almost zero, Figure 4.5(e)) due to the assistance of the adsorbed DT molecules (Figure 4.6(c)). Additionally, when the positive gate bias was applied, the injection barrier was lowered, resulting in a reduced activation energy in both contacts whereas the difference of activation energy increased at $V_{GS} < 0$ (Figure 4.6(d) and 4.6(e)). Therefore, the asymmetric current ratio had a strong dependence on the gate voltage (see Figure 4.5(f)).

4.4. Conclusion

In summary, we introduced thiol-molecules on the contact regions of a MoS₂ semiconductor surface as a tunneling paths to improve contact properties. By conducting a simple vapor treatment on MoS₂ with DT and PFDT molecular solutions, thiol-molecules were successfully chemically adsorbed at the exposed contact regions without physical damage to the electron blocking layer. The thiol-molecules created additional tunneling paths, resulting in a lower energy barrier height between the MoS₂ and metal

contacts; therefore, the primary carrier injection mechanism was changed from thermionic emission exhibiting Schottky-contact behaviors to field emission exhibiting Ohmic-contact behaviors. The contact-engineered MoS₂ FETs exhibited much better contact properties with lower activation energies and temperature-insensitive charge injection behaviors. Additionally, by depositing the thiol-molecules on only one contact region in MoS₂ FETs, asymmetric carrier injection was feasible depending on the temperature and the gate bias due to the difference in activation energy. This study presents a high-yield and simple strategy of carrier-injection engineering and can be a promising solution to improve the contact performance in MoS₂ and other 2D semiconductor FET applications.

References

- [1] B. Radisavljevic, A. Radenovic, J. Brivio, V. Giacometti, A. Kis, *Nat. Nanotechnol.* **2011**, *6*, 147.
- [2] Q. H. Wang, K. Kalantar-Zadeh, A. Kis, J. N. Coleman, M. S. Strano, *Nat. Nanotechnol.* **2012**, *7*, 699.
- [3] K. F. Mak, C. Lee, J. Hone, J. Shan, T. F. Heinz, *Phys. Rev. Lett.* **2010**, *105*, 136805.
- [4] D. Xiao, G.-B. Liu, W. Feng, X. Xu, W. Yao, *Phys. Rev. Lett.* **2012**, *108*, 196802.
- [5] Y. Yoon, K. Ganapathi, S. Salahuddin, *Nano Lett.* **2011**, *11*, 3768.
- [6] D. Jariwala, V. K. Sangwan, L. J. Lauhon, T. J. Marks, M. C. Hersam, *ACS Nano* **2014**, *8*, 1102.
- [7] Y. Zhan, Z. Liu, S. Najmaei, P. M. Ajayan, J. Lou, *Small* **2012**, *8*, 966.
- [8] C.-H. Lee, G.-H. Lee, A. M. v. d. Zande, W. Chen, Y. Li, M. Han, X. Cui, G. Arefe, C. Nuckolls, T. F. Heinz, J. Guo, J. Hone, P. Kim, *Nat. Nanotechnol.* **2014**, *9*, 676.
- [9] M. Amani, D.-H. Lien, D. Kiriya, J. Xiao, A. Azcatl, J. Noh, S. R. Madhupathy, R. Addou, S. KC, M. Dubey, K. Cho, R. M. Wallace, S.-C. Lee, J.-H. He, J. W. Ager III, X. Zhang, E. Yablonovitch, A. Javey, *Science* **2015**, *350*, 1065.
- [10] D. Jena, K. Banerjee, G. H. Xing, *Nat. Mater.* **2014**, *13*, 1076.
- [11] J. Wang, Q. Yao, C.-W. Huang, X. Zou, L. Liao, S. Chen, Z. Fan, K. Zhang, W. Wu, X. Xiao, C. Jiang, W.-W. Wu, *Adv. Mater.* **2016**, *28*, 8302.
- [12] X. Cui, E.-M. Shin, L. A. Jauregui, S. H. Chae, Y. D. Kim, B. Li, D. Seo, K. Pistunova, J. Yin, J.-H. Park, H.-J. Choi, Y. H. Lee, K. Watanabe, T. Taniguchi, P. Kim, C. R. Dean, J. C. Hone, *Nano Lett.* **2017**, *17*, 4781.
- [13] H. Kwon, W. Choi, D. Lee, Y. Lee, J. Kwon, B. Yoo, C. P. Grigoropoulos, S. Kim, *Nano Res.* **2014**, *7*, 1137.
- [14] R. Kappera, D. Voiry, S. E. Yalcin, B. Branch, G. Gupta, A. D. Mohite, M. Chhowalla, *Nat. Mater.* **2014**, *13*, 1128.
- [15] X. Cui, G.-H. Lee, Y. D. Kim, G. Arefe, P. Y. Huang, C.-H. Lee, D. A. Chenet, X. Zhang, L. Wang, F. Ye, F. Pizzocchero, B. S. Jessen, K. Watanabe, T. Taniguchi, D. A. Muller, T. Low, P. Kim, J. Hone, *Nat. Nanotechnol.* **2015**, *10*, 534.
- [16] L. Yu, Y.-H. Lee, X. Ling, E. J. G. Santos, Y. C. Shin, Y. Lin, M. Dubey, E. Kaxiras, J. Kong, H. Wang, T. Palacios, *Nano Lett.* **2014**, *14*, 3055.

- [17] S. Das, H.-Y. Chen, A. V. Penumatcha, J. Appenzeller, *Nano Lett.* **2012**, *13*, 100.
- [18] J. Kang, W. Liu, K. Banerjee, *Appl. Phys. Lett.* **2014**, *104*, 093106.
- [19] X. Duan, C. Wang, A. Pan, R. Yu, X. Duan, *Chem. Soc. Rev.* **2015**, *44*, 8859.
- [20] C. Huang, S. Wu, A. M. Sanchez, J. J. P. Peters, R. Beanland, J. S. Ross, P. Rivera, W. Yao, D. H. Cobden, X. Xu, *Nat. Mater.* **2014**, *13*, 1096.
- [21] M. Farmanbar, G. Brocks, *Phys. Rev. B.* **2015**, *91*, 161304.
- [22] M. Farmanbar, G. Brocks, *Adv. Electron. Mater.* **2016**, *2*, 1500405.
- [23] M. Makarova, Y. Okawa, M. Aono, *J. Phys. Chem. C* **2012**, *116*, 22411.
- [24] C. G. Wiegstein, K. H. Schulz, *J. Phys. Chem. B* **1999**, *103*, 6913.
- [25] S. L. Peterson, K. H. Schulz, *Langmuir* **1996**, *12*, 941.
- [26] X. Chen, N. C. Berner, C. Backes, G. S. Duesberg, A. R. McDonald, *Angew. Chem.* **2016**, *55*, 5803.
- [27] D. M. Sim, M. Kim, S. Yim, M.-J. Choi, J. Choi, S. Yoo, Y. S. Jung, *ACS Nano* **2015**, *9*, 12115.
- [28] S. Bertolazzi, S. Bonacchi, G. Nan, A. Pershin, D. Beljonne, P. Samori, *Adv. Mater.* **2017**, *29*, 1606760.
- [29] J. Kang, W. Liu, D. Sarkar, D. Jena, K. Banerjee, *Phys. Rev. X* **2014**, *4*, 031005.
- [30] A. Allain, J. Kang, K. Banerjee, A. Kis, *Nat. Mater.* **2015**, *14*, 1195.
- [31] X. Zhang, Q. Liao, S. Liu, Z. Kang, Z. Zhang, J. Du, F. Li, S. Zhang, J. Xiao, B. Liu, Y. Ou, X. Liu, L. Gu, Y. Zhang, *Nat. Commun.* **2017**, *8*, 15881.
- [32] H. Qiu, T. Xu, Z. Wang, W. Ren, H. Nan, Z. Ni, Q. Chen, S. Yuan, F. Miao, F. Song, G. Long, Y. Shi, L. Sun, J. Wang, X. Wang, *Nat. Commun.* **2013**, *4*, 2642.
- [33] K. Cho, M. Min, T.-Y. Kim, H. Jeong, J. Pak, J.-K. Kim, J. Jang, S. J. Yun, Y. H. Lee, W.-K. Hong, T. Lee, *ACS Nano*, **2015**, *9*, 8044.
- [34] C. Tsai, H. Li, S. Park, J. Park, H. S. Han, J. K. Nørskov, X. Zheng, F. Abild-Pedersen, *Nat. Commun.* **2017**, *8*, 15113.
- [35] X. Cheng, Y.-Y. Noh, J. Wang, M. Tello, J. Frisch, R.-P. Blum, A. Vollmer, J. P. Rabe, N. Koch, H. Sirringhaus, *Adv. Funct. Mater.* **2009**, *19*, 2407.

Chapter 5. Summary

In this thesis, I described the research results mainly focusing on the electrical characterization of MoS₂ field-effect transistors. The main chapters were devoted to electrical properties of MoS₂ FETs with organic thiol treatments of the surface and contact of MoS₂ devices.

First, I investigated the gate-bias stress effects on instabilities of MoS₂ based field effect transistors. The back-gated MoS₂ FETs were fabricated using electron beam lithography system. I observed threshold instability of MoS₂ FETs under various measurement conditions. After applying positive gate bias stress on the device, the threshold voltage was shifted to a positive direction and vice versa. It is found that the applied gate field could enhance or reduce stress effects, increasing or decreasing the density of adsorbed water molecules or oxygen molecules. In particular, I found the applied time dependence of threshold instability phenomena (i.e., a decrease in the difference of the threshold voltage as gate bias stress time decrease). In addition, gate bias stress effects were not observed when the measurement was conducted at the high-vacuum condition.

And secondly, electrical and optical properties of thiol-treated and untreated MoS₂ FETs were stated. The electrical properties of as made MoS₂ FETs were measured under vacuum condition. After measurements, the MoS₂ FETs were dipped into thiol molecule solvent for molecule treatment. Then, the electrical properties of thiol-treated MoS₂ FETs were measured again and compared with those of untreated devices. Also, Raman, PL and XPS were applied to confirm whether thiol molecules were adsorbed at the surface of MoS₂ or not. I fabricated 10 MoS₂ FETs having different thickness and surface/volume

ratio to investigate molecule treatment effects. It has been known that thiol molecules tend to make covalent with sulfur vacancies of MoS₂. In addition, the sulfur vacancies of MoS₂ have been considered as the dominant factors in the electrical properties of MoS₂. I observed current level reduction phenomena after organic thiol treatment. Even though current levels of thiol-treated devices were significantly reduced, the SS value of the devices was not considerably changed. This study may provide a method of modulating electrical and optoelectrical properties of MoS₂ FETs.

In chapter 4, I suggest a novel and simple way of modifying injection properties of MoS₂ FETs via selectively deposited thiol molecules. Usually, relatively complex, low-yield and difficult techniques have been required to modify contact properties. Rather than using other difficult methods, I fabricated contact-modified MoS₂ FETs by inserting thiol molecules between metal and MoS₂ only. HRTEM, XPS, and EELS were conducted for further investigation of the adsorbed thiol molecules on the surface of MoS₂. Analyses and discussions on electrical properties of contact-engineered devices were stated in chapter 4. I found that effective activation energy of the devices was successfully reduced by using this simple strategy. Also, I observed that the dominant injection mechanism was changed from thermal emission to field emission. Finally, I was able to fabricate asymmetrically contact-treated devices by using thiol treatment on only one electrode of the device. This study provides a strong strategy of contact engineering as well as a promising solution to modify the charge injection performance.

국문초록

유기 싸이올 분자 처리를 통한 이황화 몰리브덴 전계 효과 트랜지스터의 전기적 변화에 대한 연구

조경준

서울대학교 물리천문학부

그래핀이나 전이 금속 칼코겐 화합물 물질들은 새로운 특징들 덕분에 많은 주목을 받아 왔다. 그래핀의 경우 반도체 소자로서 이용하기 위한 전기적 밴드갭이 존재하지 않기 때문에, 전이 금속 칼코겐 화합물들이 차세대 소자로서 활용 가능한 이차원 적층 구조를 갖는 물질로서 많은 주목을 받고 있다. 이러한 전이 금속 칼코겐 화합물 중에서도 이황화 몰리브덴은 단분자층 일 때 1.9 eV, 다분자층 일 때 1.3 eV의 밴드갭을 가지고 있기 때문에, 큰 관심을 받게 되었다. 이러한 이유로, 많은 연구자들이 이황화 몰리브덴을 새로운 소자의 재료로서 활용하기 위해 활발한 연구를 진행해 오고 있다. 하지만, 이황화 몰리브덴의 2차원 구조적 특성 때문에 표면에서부터 전기적 특성과 광학적 특성이 큰 영향을 받게 된다. 즉, 차세대 나노 전자 소자 구현에 있어서 표면이 어떻게 이황화 몰리브덴의 특성에 어떻게 영향을 미치는지, 어떤 다양한 표면 처리 방법으로 물성을 변화시킬 수 있는지에 대한 연구가 필요한 실정이다.

이러한 측면에서, 본 학위논문에서 첫 번째로 이황화 몰리브덴 전계 효과 트랜지스터의 전기적 특성이 환경으로부터 받는 영향을 논하고자 한다. 게이트에 스트레스를 인가하는 시간의 변화, 게이트 전압의 변화 속도나 게이트 전압을 변화 시키는 범위의 변화 등, 여러 가지 측정 조건이 소자의 전기적 특성에 어떠한 영향을 미치는지에 대한 연구를 진행 하였다. 전하농도를 비롯하여, 소자의 임계 전압 값이 게이트 스트레스가 가해 졌을 때 변화 하는 것

을 확인 하였다. 양의 게이트 스트레스를 인가 하였을 때, 소자의 임계 전압이 양수 쪽으로 변화 하였고, 그 반대의 경우 역시 마찬가지였다. 이러한 효과는 게이트에서 발생하는 전기장에 의해 공기 중의 산소나 수분이 표면에 흡착 됨으로써 나타난다는 것을 실험적으로 확인할 수 있었다.

두 번째로, 유기 싸이올 분자를 이황화 몰리브덴 소자에 처리하였을 때의 전기적, 광학적 특성 변화에 대해서 기술하고자 한다. 유기 싸이올 분자들은 이황화 몰리브덴 표면에 존재하는 황 공석 자리에 화학적 결합을 하고자 하는 경향이 보고 된 바 있다. 싸이올 처리를 한 후, 물질의 결합과 관련이 있는 소자의 문턱 전압 이하 스윙 값은 큰 변화가 없었음에도 불구하고, 전류 값과 전하농도는 크게 감소 한 것을 확인할 수 있었다. 이러한 현상은 싸이올 분자가 황 공석 수를 줄임으로써 나타나는 현상이라고 사료된다.

마지막으로, 금속 전극과 이황화 몰리브덴의 접합부에 싸이올 분자 처리를 통해 전하 주입 특성을 비롯한 접합 특성을 향상시키는 연구에 대해 논의하고자 한다. 금속과의 접합부에만 싸이올 분자를 끼워 넣게 되면, 페르미 레벨의 고정을 야기하는 기존에 존재하던 계면의 결합들을 없애는 동시에 전하 주입 장벽을 줄일 수 있다는 것을 확인 하였다. 소자의 활성 전위가 낮아지고, 상온에서조차 쇼트키 접합 특성을 보이던 소자가, 저온에 이르기까지 오믹 접합 특성을 보이는 것을 확인할 수 있었다. 이러한 방법을 사용하여, 비 대칭적인 접합 특성을 갖는 소자의 제작 또한 구현이 가능함을 확인하였다.

Keywords: 이 차원 물질, 전이 금속 칼코젠 화합물, 이황화 몰리브덴, 전기적 특성, 게이트 스트레스 인가 효과, 계면 조절, 싸이올 분자 처리

Student Number: 2012-20388

감사의 글

제게 있어서 대학원은 2012년 3월부터 지금 글을 적고 있는 이 순간까지 제 인생에 가장 오래 머물렀던 공간입니다. 오랜 기간이었던 만큼 많은 경험들을 할 수 있었고, 이러한 경험들로부터 많은 것을 새롭게 배울 수 있었고, 아직도 부족하지만 부족했던 저의 많은 것을 바꾸게 되었습니다. 쉽지 않은 대학원 생활이었던 만큼 감사한 많은 분들 덕분에 여기까지 무사히 올 수 있었다고 확신하며 감사의 말씀 드립니다.

가장 먼저 지도교수님이신 이택희 교수님께 진심으로 감사 드립니다. 제 인생의 가장 큰 변화였던 대학원 생활과 결혼식의 주례까지, 늘 함께 해주셨던 교수님의 인자하신 성품과 지도 덕분에 부족한 제가 그래도 여기까지 올 수 있었던 것 같습니다. 아직도 많이 부족하지만 앞으로 교수님의 명성에 누가 되지 않는 제자가 될 수 있도록 끊임없이 노력하겠습니다. 항상 행복하시고 건강하시길 바라겠습니다.

그리고 오랜 시간 함께 해 준 즐거운 MNELAB 구성원 여러분께도 감사의 말씀 전하고 싶습니다. 처음 연구실에 들어온 순간부터 연구실의 어머니 같은 존재였던 현학이 형. 착한 성품과(비록 저를 LOL의 세계로 인도했지만) 인자한 웃음, 부지런하고 꾸준히 연구하는 형의 모습을 보며 많은 것을 배우고 느꼈습니다. 미국에서 행복하게 잘 지내시길 바랍니다. 그리고 다른 학교에서 와 아무것도 모르던 제게 MNELAB을 소개해준, 어쩌면 지금의 저를 있게 만든 진곤이 형에게도 감사의 말씀 전하고 싶습니다. 형과 함께 톨루엔 뚜껑을 가위로 따다가 글러브 박스 장갑을 바꿔 낀 것이 어제 같은데 벌써 제가 졸업을 하게 되었습니다. 항상 건강히 잘 지내시기 바랍니다. 그리고 연구실의 분위기 메이커 marine988 동구 형. 왕택이와 함께 클린룸 장비를 배우던 게 벌써 7년전이라는게 믿기지 않네요. 회사 생활 항상 힘내시고 건강하시기 바랍니다. 연구실 동기로 들어왔던 한기 형. 비록 지금은 다른 분야에 계시지만, 그 쪽에서도 잘 하시는 모습을 보니 저도 기분이 좋고 앞으로도 계속 승승장구하시기 바랍니다. 2D 팀 든든한 만형이셨던 태영이 형. 형이 2D 팀 팀장이자 방장으로 계시면서 많은 일을 해 주셔서 2D 팀 사람들이 고생 없이 즐겁게 생활할 수 있지 않았나 싶습니다. 육아로 힘들고 바쁘실 텐데 파이팅 하시기 바랍니다. 함께 협곡을 누비던 영걸이 형. 형의 빛나던 냉철한 지성과 대비되는 탐 라이너로서의 모습 감명 깊었습니다. 회사 생활 늘 파이팅 하시고 최근 바쁘실 텐데 모두 탈 없이 행복하게 마무리 되길 바랍니다. 연구실 멤버 중 처음으로 동갑이었던 왕택이. 형들뿐이던 연구실에 처음으로 친구가 들어와서 알게 모르게 심적으로 위안이 많이 되었던 것 같다. 하던 연구 마무리 잘 되어서 좋은 일만 있길 바란다. MNE 핵인싸 대경이 형. 제가 착한 형에게 장난을 너무 많이 한 건 아닌지 모르겠네요. 청춘 사업 성공하시길

바라고 하시는 연구도 늘 잘 되길 바라겠습니다. 2D팀의 든든한 기둥인 진수 형. 형이 계셔서 제가 정말 편하게 연구실 생활 할 수 있었던 것 같습니다. 늘 많은 도움 주셔서 감사하고 앞으로도 늘 행복하시길 바라겠습니다. 분자팀의 똑똑한 연식이. 아직도 비오는 날 한 손에 우산을 들고 슬라이퍼를 신고 전기 자전거를 타며 유유히 지나가던 너의 모습이 눈앞에 선하다. 원하는 길 찾아서 후회 없고 행복하게 지내길 바라. 성실함의 대명사 영록이 형. 늘 묵묵히 311호를 지키며 일 하시는 모습을 보며 나태한 제 자신의 모습을 돌아보며 많이 반성하게 되는 계기가 되었습니다. 알게 된지 벌써 10년 된 재근이. 갓재근은 갓갓갓이라 걱정이 별로 안된다. 앞으로 2D 팀 팀장이 되어 어깨가 무거울텐데 지금처럼 열심히 연구하고 항상 좋은 결과 있길 바라고 여자친구 랑도 행복하게 잘 지내길 바란다. 곧 유부남이 될 우철이 형. 결혼 해보니까 좋은거 같아요. 형도 결혼 준비 중이라 바쁘겠지만, 마무리 잘 하시고 다미씨와 함께 행복하게 사시길 바랍니다. 그리고 준우 더 리치 김 형. 힘든 대학원 생활 잘 마무리 하시고 꼭 꿈을 이루시길 바라겠습니다. 회사로 간 유리도 항상 건강하고 행복하게 지내길 바라. 늘 밝고 긍정적인 지원이. 힘든 대학원 생활이지만 좋은 사람들과 함께라면 잘 헤쳐 나갈 수 있을 거라 믿어. 나랑 같이 졸업하는 정민이도 어디에서 무슨 일을 하더라도 행복하게 지내길 바라. 얼마 전까지 막내였던 재영이와 희범이도 늘 잘 지내고 대학원 잘 마치길 바란다. 연구실 새로운 막내 민우. 빠릿빠릿한 신입생이라 잘 헤쳐나 갈거라 생각되고 웃는 모습으로 졸업하길 바란다. 그리고 젠틀남 영국 신사 기훈이 형. 제가 이제 학교를 떠나게 되어 기과연 트리오에서 탈퇴하지만 남은 기과연 듀오끼리 연구 잘 하셔서 (재근이를 갈귀서) 원하는 것 꼭 이루시길 바라겠습니다. 좋은 연구도 함께 했으면 좋겠네요. 역시 제가 아무것도 모르던 시절 많은 것을 알려주신 홍웅기 박사님께도 감사의 말씀 전하고 싶습니다. 마지막으로 정말 많은 가르침과 도움을 받았던 승준이 형. 아직 부족한 저 때문에 많은 고생 하고 계신데, 늘 선뜻 도와 주시고 많은 가르침 주셔서 감사합니다. 아낌없는 조언들로부터 아직도 많이 배우고 있습니다. 남은 일들도 함께 잘 마무리 할 수 있으면 좋겠습니다.

이와 더불어 대학원 생활을 더 잘 견딜 수 있게 해준 경북과고 친구들에게도 감사의 말씀 전하고 싶습니다. 항상 어그로 끌지만 누구보다 여리고 착한 성경이, 무릎 운전 마스터 규철이, 고집불통 환상의 바텀듀오 태훈이, 같은 과지만 보기 힘든 진욱이도 힘든 대학원 생활 잘 마치기 바란다. 전문직 개인 변호사 훈찬이, 경북과고 주치의 환주는 전문직이기 때문에 뭐... 별 걱정 없고 잘 할거라고 생각된다. FPS 마스터 중엽이, 징징이 우현이, 시크한 대영이 모두 준비 하는 일 잘 풀려서 2019년 행복한 한해 되길 바란다. 그 외에도 여기에는 다 적지 못했지만 힘든 대학원 생활에 많은 위안이 되었던 우리 경북 과고 친구들에게 진심으로 감사한 마음입니다. 또 중학교 때부터 늘 만났던, 나보다도 훨씬 더 의젓한 기혁이. 너의 소신과 꿈 항상 응원하고 아내와 함께 꼭 꿈 이뤄서 행복하게 지냈으면 좋겠다. 그 외에 언급 못한 친구들

모두 각자의 자리에서 하는 일 잘 되어서 지금처럼 좋은 친구로 남았으면 좋겠습니다.

그리고 지금 이 순간까지 부족한 큰아들을 부족함 없이 사랑으로 키워 주신 부모님과 사랑하는 동생 경욱이에게도 무한한 감사의 말씀 드리고 싶습니다. 항상 무뚝뚝하고 표현도 잘 안하고 짜증 많은 큰아들이지만, 속으로는 늘 무한한 감사와 애정을 가지고 있다는 것을 부끄럽지만 이 자리를 빌어 이야기 해봅니다. 앞으로도 늘 건강하게 오래 저의 든든한 버팀목이 되어 주셨으면 좋겠습니다. 저 때문에 걱정 많으셨을텐데 이제 결혼도 했으니 저 또한 한 가정의 가장으로서 부모님 이름에 부끄럽지 않게 의젓하게 나아가며 효도하는 아들이 되겠습니다. 또, 하나뿐인 동생 경욱이. 어릴 때는 많이 싸우기도 했지만, 이제는 둘도 없는 든든한 동생이 되어 줘서 정말 고맙다. 전역 하고 나서도 하고 싶은 일 잘 찾아서 행복하게 살길 바란다. 또한 손주 늘 걱정 해주시고 신경 써주시는 할머니와 외할머니 모두 정말 감사하다는 말씀 드리고 싶고, 늘 건강 잘 챙기시고 오래오래 행복하시길 바랍니다. 그리고 저를 믿고 아껴주시는 장인어른, 장모님 항상 감사합니다. 사랑하시는 딸 가현이 행복하게 잘 살 수 있도록 늘 제가 옆에서 지켜 주고, 함께 행복하게 살아가는 모습 보여 드리겠습니다. 용산도 자주 찾아 뵙고 효도하며 살겠습니다. 늘 건강하고 행복하시고 오래오래 저희 곁에서 든든한 버팀목이 되어 주셨으면 좋겠습니다. 그리고 항상 신경 써 주시는 친가/외가 친척 어른들께도 감사 인사 드리고 싶습니다.

마지막으로 사랑하는 아내 가현이에게 무한한 감사 표하고 싶습니다. 2011년 3월부터 오랜 연애 기간의 대부분을 대학원 생활 한다는 핑계로 많이 챙겨 주지 못해서 미안하고, 내 인생에 가장 잘 한일이 있다면 여보와 결혼 한 일이 아닐까 싶어. 항상 나를 믿고 사랑해줘서 고맙고, 앞으로도 남은 인생 평생 서로 아끼고 행복하게 살자. 앞으로 힘든 인턴, 레지던트 기간이 남았는데 서로 힘내서 잘 견뎌내고 나면 서로 서로 더 성숙한 사람이 되어 있지 않을까 싶어. 늘 행복하고 건강하게 오래오래 함께 살자.

어떻게 보면 대학원이라는 온실을 떠나며, 망망대해를 눈 앞에 두고 있는 심정입니다. 인생의 큰 분기점을 맞이하며 감사한 여러분들께 감사의 인사를 이렇게나마 드릴 수 있게 되어서 다행입니다. 앞으로도 늘 겸손하고 성실하게, 사소한 것들에 감사하며 행복하게 잘 살겠다고 늘 제 옆에서 지켜 봐 주시는 여러분들께 약속 드리며 이만 줄이겠습니다.